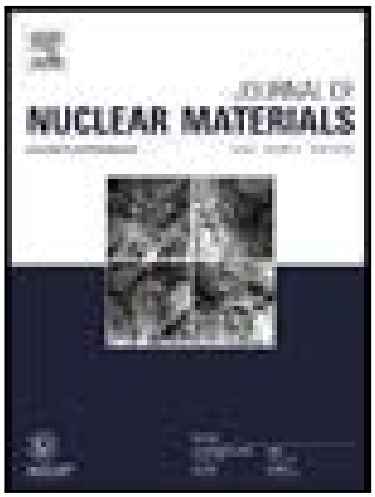

Tungsten–Tantalum Alloys for Fusion Reactor Applications

Shuhei Nogami , Itsuki Ozawa , Daisuke Asami , Naoya Matsuta , Seiji Nakabayashi , Siegfried Baumgärtner , Philipp Lied , Kiyohiro Yabuuchi , Takeshi Miyazawa , Yuta Kikuchi , Marius Wirtz , Michael Rieth , Akira Hasegawa

PII: S0022-3115(22)00228-8
DOI: https://doi.org/10.1016/j.jnucmat.2022.153740
Reference: NUMA 153740

To appear in: *Journal of Nuclear Materials*

Received date: 10 December 2021
Revised date: 14 April 2022
Accepted date: 19 April 2022

Please cite this article as: Shuhei Nogami , Itsuki Ozawa , Daisuke Asami , Naoya Matsuta , Seiji Nakabayashi , Siegfried Baumgärtner , Philipp Lied , Kiyohiro Yabuuchi , Takeshi Miyazawa , Yuta Kikuchi , Marius Wirtz , Michael Rieth , Akira Hasegawa , Tungsten–Tantalum Alloys for Fusion Reactor Applications, *Journal of Nuclear Materials* (2022), doi: https://doi.org/10.1016/j.jnucmat.2022.153740

Tungsten–Tantalum Alloys for Fusion Reactor Applications

Shuhei Nogami[1], Itsuki Ozawa[1], Daisuke Asami[1], Naoya Matsuta[2], Seiji Nakabayashi[2], Siegfried Baumgärtner[3], Philipp Lied[3], Kiyohiro Yabuuchi[4], Takeshi Miyazawa[1], Yuta Kikuchi[1], Marius Wirtz[5], Michael Rieth[3], Akira Hasegawa[1]

[1] Department of Quantum Science and Energy Engineering, Graduate School of Engineering, Tohoku University, 6-6-01-2, Aramaki-aza-Aoba, Aoba-ku, Sendai 980-8579, Japan

[2] A.L.M.T. Corp., 2, Iwasekoshi-machi, Toyama 931-8543, Japan

[3] Institute for Applied Materials, Karlsruhe Institute of Technology, Hermann-von-Helmholtz-Platz 1, 76344 Eggenstein-Leopoldshafen, Germany

[4] Institute of Advanced Energy, Kyoto University, Gokasho, Uji, Kyoto 611-0011, Japan

[5] Institute for Energy and Climate Research, Forschungszentrum Jülich GmbH, 52425 Jülich, Germany

Corresponding Author

Name Shuhei Nogami

Postal address Department of Quantum Science and Energy Engineering, Graduate School of Engineering, Tohoku University, 6-6-01-2, Aramaki-aza-Aoba, Aoba-ku, Sendai 980-8579, Japan

Telephone +81-22-795-7923

Fax number +81-22-795-7924

E-mail address shuhei.nogami.d3@tohoku.ac.jp

Abstract

Tungsten–tantalum (W-Ta) alloys containing 1–5%Ta were developed for fusion reactor applications. For the mechanical properties and resistance against recrystallization in the non-irradiated state, Ta-alloying improved the performance of W. Grain refining and solute Ta improved the recrystallization temperature and strength. In addition, W-1%Ta exhibited a superior ductility, including ductile-to-brittle transition temperature (DBTT), which might be attributed to the strength of sub-grain boundary. Proton irradiation study at 1500 °C to 0.5 dpa revealed a decrease in irradiation hardening (increase in hardness) in recrystallized specimens and a decrease in hardness reduction in as-received specimens with increasing Ta concentration. With respect to the high temperature irradiation of the as-received specimens, microstructural recovery followed by recrystallization could be one of the dominant factors affecting the hardness change. As a material performance required for the actual components of fusion reactors, resistance against high heat flux exposure have been studied through thermal shock tests. Thorough this experiment, it was clarified that the degradation by high heat flux exposure could be suppressed due to Ta-alloying.

Keywords:

Tungsten, Tantalum, Alloying, Mechanical property, Irradiation hardening

1. Introduction

Brittleness at low temperature [1–9], recrystallization-induced embrittlement [10–13], and neutron-irradiation-induced embrittlement [14–17] are some of the drawbacks associated with tungsten (W) when applied to fusion reactors. In addition, the intrinsic brittleness of W results in its poor workability. It is known that the brittleness of W is mainly attributed to the absence of close-packed planes and week grain boundary strength. To overcome these drawbacks, grain refining [18], work hardening [19], solid solution alloying [20, 21], and dispersion strengthening [21, 22], have been applied to W materials. For solid solution alloying, rhenium (Re) is one of the most effective elements [20, 21]. According to the previous study [23], W materials alloyed by Re exhibited a better ductility and workability than pure W, which could be induced by the improved dislocation mobility [24, 25], grain refining [26], and an increase in the recrystallization temperature [27] by solute Re. For dispersion strengthening, oxide and carbide particles, such as yttria (Y_2O_3) [28], lanthanum oxide (La_2O_3) [29, 30], titanium carbide (TiC) [31, 32], tantalum carbide (TaC) [33], and zirconium carbide (ZrC) [34], with sizes ranging from nm to μm, have been used as dispersants. In contrast to such solid particle cases, W dispersion strengthened by potassium (K) bubbles, known as K-doped W, is also well known as a dispersion strengthened W material with improved mechanical properties [22]. Because the movement of grain boundaries and dislocations could be suppressed by these dispersants, dispersion strengthening could be realized in addition to grain refining and inhibition of recrystallization [22, 35–37].

In our previous studies, as well as the grain refining and work hardening, K-doping and/or Re-alloying have been applied to powder-metallurgical-processed W, which was finalized by a hot-rolling or swaging accompanied by a stress-relief heat treatment. After evaluating the K-doped and/or 3%Re-alloyed W plates and rods, whose major production

conditions (cold isostatic pressing (CIP), sintering, rolling/swaging, and heat treatment) were the same, K-doping and/or Re-alloying exhibited positive effects in the non-irradiated state. K-doped W, W-3%Re, and K-doped W-3%Re alloys demonstrated increased resistance to recrystallization, strength and ductility, ductile-to-brittle transition temperature (DBTT), and the other various properties compared to pure W [38–54]. After neutron irradiation in the temperature range of 600–1000 °C to 0.5 dpa with no production of solid transmutation elements, hot-rolled plates made of the three alloys demonstrated no significant degradation of tensile properties [55, 56]. However, for neutron irradiation in the temperature range of 600–1100 °C to 1 dpa with a certain level of production of transmutant Re and osmium (Os), the irradiation-induced embrittlement (increase in DBTT) of K-doped W-3%Re occurred, whereas K-doped W exhibited a suppressed degradation [57]. It is possible that the enhanced formation of irradiation-induced/enhanced precipitates and solute-rich clusters caused the embrittlement [57–73].

To avoid the possibility of embrittlement enhanced by solid transmutation, alloying by a complete solid solution element in W might be a better choice. According to the binary phase diagrams, tantalum (Ta), vanadium (V), niobium (Nb), and molybdenum (Mo) fall into this category [74]. From the perspective of induced radioactivity, it is considered in general that the use of Nb and Mo should be avoided in the fusion reactors [75, 76]. In contrast, although Ta and V do not have such intrinsic issues, no clear improvement in ductility (decrease in DBTT) owing to Ta- and V-alloying was observed according to the previous studies [77, 78]. W-5%Ta and W-5%V forged materials exhibited a brittle fracture by Charpy impact tests, even at 1000 °C, whereas the forged pure W obtained through the same production route exhibited a ductile fracture above 700 °C [77]. In contrast, W-1%Ta obtained through the same production route exhibited a ductile fracture above 700 °C, however no significant improvement compared to the pure W was observed [77]. In addition,

the fracture toughness of forged W-Ta alloys evaluated by the three point bending tests was not improved due to the change in Ta concentration from 1 to 10 % [78]. Based on these previous studies and other related studies, W-Ta and W-V alloy systems were not considered promising for fusion reactor applications [79, 80]. However, the thermo-mechanical properties of most alloyed materials might be influenced not only by the solid solution alloying itself but also by the fabrication methods and conditions. Therefore, the thermo-mechanical properties of materials with the same major chemical composition could be controlled by the fabrication methods and conditions. According to our previous studies [46, 49, 53], pure W and K-doped and/or Re-alloyed W fabricated by various methods (e.g., hot-rolling or swaging) and under various conditions (e.g., reduction ratio in rolling and swaging) exhibited different strength and ductility by tensile test, DBTT and upper shelf energy (USE) by Charpy impact test, and recrystallization and grain growth behaviors, even if the major chemical composition and concentration of dispersant were the same.

In the present study, hot-rolled W plates alloyed by Ta with various concentrations were developed to re-investigate the availability of W-Ta alloy system for fusion reactor applications. In addition to the thermo-mechanical properties with no irradiation effects, the irradiation response (microstructure evolution and irradiation hardening) was evaluated by using an accelerator-based ion irradiation. In addition to the W-Ta alloy plates, pure W and W-3%Re alloy plates, whose major conditions of material fabrication were the same as those of W-Ta alloys, were also investigated for comparison. Some of the properties of pure W and W-3%Ta in the non-irradiated state were previously obtained, having been reported in open literature [38, 39, 46, 47, 49–53, 81].

The previous irradiation studies using ion irradiation have reported the microstructure evolution, irradiation hardening, and effect of helium, where not only W-Ta but also W-Re and W-Re-Ta alloys were examined to clarify the individual and simultaneous

effects of solute Ta and Re [82–89]. The ion irradiation in the temperature range of 300–750 °C induced the formation of dislocation loops in pure W, W-5%Ta, and W-5%Re alloys [83, 86, 87]. In this temperature range, higher number density and smaller size of dislocation loops were observed in the W-5%Ta alloy compared to in pure W. After the irradiation increased to higher doses, irradiation-induced clustering of Re occurred in W-2%Re and W-2%Re-1%Ta alloys, whereas no clustering was observed in W-4.5%Ta. In the W-2%Re-1%Ta alloy, the number density and volume fraction of Re clusters were lower than those of W-2%Re alloy, which resulted in a suppressed irradiation hardening [82, 84, 85]. In contrast, high temperature irradiation and post-irradiation annealing at temperatures above 800 °C induced the formation of voids in pure W and W-5%Ta alloy [86, 88]. In this temperature range, the vacancy mobility and void formation were suppressed by Ta-alloying, which was explained by a solute-vacancy trapping mechanism. Most previous irradiation studies on the microstructure and irradiation hardening examined the arc-melted and annealed materials (e.g., materials consisted of the recrystallized grains accompanied by very low number density of dislocations) at irradiation temperatures below 1000 °C. In the present study, not only recrystallized but as-produced (just after the hot-rolling accompanied by stress-relief heat treatment) materials were examined at irradiation temperatures above 1000 °C, which was aimed at simulating the actual temperature condition of a fusion reactor component, for instance, divertors.

2. Experimental

2.1 Materials and microstructure characterization

W plates alloyed by 1%, 3%, and 5%Ta, whose fabrication was ordered to A.L.M.T. Corp., were used to clarify the effects of Ta-alloying. Powder metallurgy (CIP and sintering) and hot rolling followed by stress-relief heat treatment were applied to these materials.

Hereinafter, the materials after these procedures are referred to as materials in the as-received condition.

Concentrations of alloying elements (Ta and Re) and interstitial impurity atoms (carbon (C), nitrogen (N), and oxygen (O)) in pure W, those three W-Ta alloys, and W-3%Re alloy are summarized in Table 1. Although it was concerned that such interstitial impurities might influence the movement of grain boundaries, and other material behaviors owing to their segregation at grain boundaries, the concentration of O in W-Ta alloys was slightly higher than the level (<10 ppm) of W materials examined in the previous studies [51, 53]. Because the chemical affinity between Ta and O is known to be high, it was possible that a slight contamination of O occurred during the fabrication process (e.g. CIP, sintering, and hot-rolling).

The grain structure and grain size of the W-Ta alloys were investigated on the L × S surface after mechanical polishing, followed by electrolytic polishing. The definitions of the L, T, and S directions are shown in Fig. 1 (a). The grain sizes were measured based on the ASTM E112-85 standard using metallographic optical microscope images after polishing [90]. In addition, microstructural observations were performed using a transmission electron microscope (TEM) with a thin foil specimen produced by electrolytic polishing using a single jet apparatus. Furthermore, X-ray diffraction (XRD) analysis was performed to evaluate the lattice constants of the pure W and W-Ta alloys in the as-sintered condition.

2.2 Annealing and hardness measurement

The recrystallization behavior of W-Ta alloys was evaluated through an isochronal annealing for 1 h in the temperature range of 1200–2300 °C. Vickers hardness was measured on the L × S surfaces of the annealed materials (load: 1.96 N, dwell time: 15 s). The same method as discussed in the previous section was used for grain size measurement after

annealing.

2.3 Tensile test

Tensile tests of W-Ta alloys were performed at temperatures ranging from room temperature to 1300 °C in vacuum at a strain rate of 1×10^{-3} s^{-1}. An SS-J type specimen aligned along the L direction was used. The gauge length, gauge width, and thickness of the specimen were 5, 1.2, and 0.5 mm, respectively (see Fig. 1 (b)). As tensile properties, ultimate tensile strength (UTS), 0.2% proof stress ($\sigma_{0.2}$), uniform elongation (UE), total elongation (TE), and reduction in area (RA) were evaluated. The ruptured specimens were observed using a scanning electron microscope (SEM) to evaluate the RA and fracture manner. Because the cross-head displacement was controlled in the tensile tests, the strain values obtained in the present study (cross-head displacement/gauge length) would be larger than the actual strain in gauge section.

2.4 Charpy impact test

Charpy impact tests of W-Ta alloys were performed at temperatures below 1000 °C in vacuum, which were based on the EU standard DIN EN ISO 14556:2017-05 [91]. A KLST Charpy V-notched specimen aligned along the L-S direction was used. The length, width, height, notch depth, and notch root radius of the specimen were 27, 3, 4, 1, and 0.1mm, respectively (see Fig. 1 (c)). The span of the lower-die of the testing machine was 22 mm. The definition of the L-S direction is shown in Fig. 1 (a). As Charpy impact properties, absorbed energy, USE, and DBTT were evaluated.

2.5 Proton irradiation and post-irradiation experiments

Irradiation tests of pure W, W-Ta alloys, and W-3%Re alloy in the as-received and recrystallized (annealed for 1 h at temperature of 2300 °C) conditions were performed using a 3 MeV proton beam from the 4.5 MV Dynamitron accelerator at Tohoku University. Fig. 2 shows the distribution of displacement damage (unit in dpa) in W-5%Ta after 3 MeV proton irradiation calculated using the SRIM-2013 (The Stopping and Range of Ions in Matter) code [92]. The value and distribution of the displacement damage did not vary significantly with the concentrations of Ta and Re. For this calculation, the threshold displacement energies of W and Ta were assumed to be 90 eV [93]. The displacement damage of the uniformly irradiated region was approximately 0.5 dpa, which ranged from the specimen surface to a depth of approximately 15 μm. The irradiation temperature was 1500 °C. The L × T surface was irradiated.

After the ion irradiation, Vickers hardness measurements were performed on the irradiated surface to evaluate the irradiation hardening (load: 0.49 N, dwell time: 15 s). Microstructural observations of pure W and W-5%Ta were performed using a TEM on a thin foil specimen, which was produced through electrolytic polishing using a single jet apparatus. Specimens were thinned from the proton-irradiated side until they reached the depth for observation (approximately in the range of 3–5 μm from the specimen surface) and subsequently polished on the backside until the thickness became suitable for the TEM observation.

2.6 Thermal diffusivity measurement

The heat removal capability is important for the plasma-facing materials of fusion reactor high-temperature components such as divertors. Thus, thermal properties were evaluated as well as the aforementioned mechanical properties. In general, the thermal conductivity of alloyed materials is lower than that of pure material. Therefore, the

modification of W materials by solid solution alloying could degrade their thermal properties. Thus, balancing thermal and other properties is important for the development of new materials. In the present study, thermal diffusivity was measured to investigate the thermal properties of W-Ta alloys. The measurements were performed along S direction at temperatures ranging from room temperature to 500 °C in argon using a xenon flash apparatus. Disk-shaped specimens with a diameter of 10 mm and thickness of 2 mm were prepared for these measurements. Correlation of the raw data was performed according to Cowan et al. [94].

3. Results and Discussion

3.1 Microstructure

The grain structures observed on the L × S surface of pure W and W-Ta alloys through an optical microscope are shown in Fig. 3. Most W materials, which are fabricated through rolling, exhibits elongated grains along the rolling (L) direction. The grains are surrounded by high-angle grain boundaries (HAGBs). As well as these materials, the materials used in the present study exhibited elongated grains along the L direction, as indicated by chemically etched metallographic images shown in Fig. 3. Such worked W materials consist of grains surrounded by HAGBs and cells in the grains. The cell walls consisted of tangled dislocations, which are low-angle grain boundaries (LAGBs). The average sizes of grains surrounded by HAGBs of the pure W and W-Ta alloys in as-received condition, which were measured along the L and S directions, are summarized in Fig. 4. The average sizes of grains along L and S directions decreased with Ta concentrations; 106 and 28 μm for pure W, 64 and 14 μm for W-1%Ta, 53 and 13 μm for W-3%Ta, and 51 and 12 μm for W-5%Ta. The TEM images shown in Fig. 5 indicate the cells in the grains. The average sizes of cells of the pure W, W-1%Ta, and W-3%Ta in as-received condition were approximately 2,

1.5, and 1.4 μm, respectively. As shown in Figs. 8 (a) and (b), 1%Ta-alloying caused significant refining of grains and cells, however, only a slight decrease in these sizes was induced by increasing the Ta concentration to 5%. The refining of grains and cells might be caused by the suppressed movement of grain boundaries and dislocations by solute Ta.

Precipitates were randomly formed in W-3%Ta (Fig. 5 (c)), whereas no such precipitates were observed in pure W (Fig. 5 (a)) and W-1%Ta (Fig. 5 (b)). The XRD analysis of pure W and W-Ta alloys in the as-sintered condition revealed no signals indicating precipitates such as oxides. To discuss the solution status of Ta in pure W and W-Ta alloys, the lattice constants were evaluated using the XRD analysis results. First, the lattice constant, a, was determined as expressed by the following equations for each peak of the XRD analysis;

$$a = d\cdot(h^2 + k^2 + l^2)^{1/2} \quad (1)$$

$$d = \lambda/(2\sin\theta), \quad (2)$$

where d denotes the lattice plane spacing, h, k, and l are the miller indices, λ is the wavelength (1.540598 Å for CuKα), and 2θ is the diffraction angle. Thereafter, the lattice constants were plotted against the Nelson-Riley's function, $1/2\cdot(\cos2\theta/\sin\theta + \cos2\theta/\theta)$. By extrapolating this relation to $\theta = \pi/2$, the lattice constant a of each material was determined. Fig. 6 shows the relationship between the lattice constant and Ta concentration of the pure W and W-Ta alloys. In this figure, the theoretical relation calculated by the following equation based on Vegard's law was also plotted as a dotted line [95]:

$$a = a_W\cdot N_W + a_{Ta}\cdot N_{Ta}, \quad (3)$$

where a_W (3.1648 Å) and a_{Ta} (3.2960 Å) denote the lattice constants of W and Ta, and N_W and N_{Ta} denote the molar fractions of W and Ta, respectively. According to a comparison between the experimental and theoretical lattice constants, most of the Ta atoms in W-Ta alloys in the as-sintered condition could exist as a solid solute. Therefore, it is possible that the precipitates observed in the W-3%Ta alloy shown in Fig. 5 (c) could be formed during fabrication processes after the sintering (during hot-rolling and heat treatment for stress relief, etc.). Based on the TEM and XRD results, the number density of the precipitates could be very small. Therefore, the effect of precipitates on the thermo-mechanical properties might not be significant. Unfortunately, no evaluation of the lattice constant of materials after sintering could be performed because of the low accuracy, probably owing to plastic deformation introduced during hot-rolling.

Vickers hardness in the as-received condition were 480 for pure W, 513 for W-1%Ta, 518 for W-3%Ta, and 538 for W-5%Ta (see Fig. 7). These results indicated that solid solution strengthening by Ta occurred. As shown in Fig. 8 (c), a clear increase in hardness with addition of 1%Ta and a further slight increase with addition of 3–5% occurred. The behavior of hardness change dependent on Ta concentration was similar for both the as-received and recrystallized materials. Therefore, the difference in hardness between the as-received and recrystallized materials (ΔHV =100–110) could be attributed to the dislocations and cells formed during fabrication (hot-rolling, etc.) and their densities might not vary with Ta concentration.

3.2 Microstructural recovery and recrystallization

Vickers hardness change shown in Fig. 7 (a) indicated a microstructural recovery followed by recrystallization of pure W and W-Ta alloys during isochronal annealing up to 2300 °C for 1 h [49, 51, 53, 81]. The recrystallization temperature, which was determined as

the temperature immediately after the steep reduction in hardness, was 1250 °C for pure W, 1600 °C for W-1%Ta, 1650 °C for W-3%Ta, and 1650 °C for W-5%Ta. Based on these results, Ta-alloying could improve the resistance to recrystallization, which might be caused by the suppressed movement of grain boundaries and dislocations by solute Ta. As shown in Fig. 7 (b), the effect of 1%Ta-alloying on the recrystallization temperature was significant, however, Ta concentrations ranging from 1 to 5% induced slight difference. In contrast, the hardness reduction owing to microstructural recovery was more significant when the Ta concentration was lower.

3.3 Mechanical properties

The effect of test temperature on the tensile properties of pure W and W-Ta alloys in the as-received condition along L direction is shown in Fig. 9 [38, 39, 49–51, 53, 81]. Ta-alloying induced an increase in strength (UTS and $\sigma_{0.2}$) at all test temperatures (see Figs. 9 (a) and (b)). As well as the Ta concentration dependences of grain size and hardness (see Fig. 8), the strength clearly increased with addition of 1%Ta and a further slight increase by addition of 3–5%Ta occurred. Thus, the increase in strength might be caused by the grain refining and solid solution strengthening by Ta.

In contrast, ductility (TE and RA) of W-Ta alloys was similar to or lower than that of pure W, except for the W-1%Ta alloy tested at 100 °C (see Figs. 9 (c) and (d)). At 100 °C, W-1%Ta exhibited 13% TE and 25% RA, whereas the other materials exhibited no TE and RA. As shown in Fig. 10, the surface of the test section of specimens after tensile test exhibited plastic deformation with slip lines in the test temperature range, where elongation was detected. The area showing visible slip lines tended to extend with a decrease in the test temperature. Considering our previous study [39], this phenomenon could be explained based on the relationship between strain rate and dislocation velocity. As well as the present study, a

previous study on K-doped W plate indicated that the area occurring plastic deformation with slip lines increased with an increase in the strain rate and decrease in the test temperature, and these phenomena were explained by the relationship between the strain rate and dislocation velocity. If the strain rate was constant, the mobile dislocation density could increase with a decrease in temperature.

For the tensile tests at 100 °C, the effect of Ta concentrations ranging from 1 to 5% induced a difference in ductility and macroscopic deformation behaviors. In contrast, the fracture surfaces exhibited the same fracture manner, as shown in Fig. 11. All four materials exhibited brittle cleavage fractures at 100 °C. For the tensile tests at 200 °C, no significant difference in ductility and macroscopic deformation behaviors were observed among the materials. In contrast, W-1%Ta and W-3%Ta exhibited a brittle cleavage fracture, whereas pure W and W-1%Ta exhibited a ductile fracture. The ductility, deformation behavior, and fracture manner could be dominated by several factors such as material features, test temperature, strain rate, and specimen shape. Further investigations are necessary to clarify the mechanism of these phenomena and the effect of Ta concentration.

The lower strength (UTS and $\sigma_{0.2}$) and higher ductility (TE and RA) of pure W were observed at temperatures ranging from 1100 to 1300 °C compared to W-Ta alloys. It is known that recrystallized W materials could exhibit the lower strength and higher ductility, which is attributed to the low dislocation density [96, 97]. According to the present study on isochronal annealing, the recrystallization temperatures of pure W and W-Ta alloys were 1250 °C and ranged from 1600 to 1650 °C, respectively. Therefore, the lower strength and higher ductility of pure W compared to the W-Ta alloys could be due to recrystallization. For the W-Ta alloys, the RA decreased at temperatures ranging from 900 to 1300 °C, which could be attributed to the enhanced grain boundary sliding and crack formation with test temperature, as shown in Fig. 12. Because the number density and opening width of cracks

formed in W-5%Ta alloys were larger than those of W-1%Ta and W-3%Ta, the RA of W-5%Ta at 1300 °C was lower than that of W-1%Ta and W-3%Ta. Related to these results, dimple density in the fracture surface of W-5%Ta was smaller compared to W-1%Ta and W-3%Ta (see Fig. 11). In contrast to the W-Ta alloys, no such grain boundary sliding and crack formation were observed in pure W at 1300 °C. Similar to the W-Ta alloys in the present study, a reduction in RA accompanied by the grain boundary sliding and crack formation was observed in K-doped W-3%Re after tensile tests at 1500 and 1800 °C [98]. Based on these results, it was considered that the dominant factor in the deformation of W materials could be changed from a transgranular plastic deformation to grain boundary sliding and crack formation with increasing test temperature. Although one condition of strain rate was applied in the present study, the mechanism of high temperature deformation (e.g., dislocation motion and grain boundary sliding) would vary even with the strain rate [99].

The effect of test temperature on the Charpy impact properties of pure W and W-Ta alloys in the as-received condition along L-S direction is shown in Fig. 13 [46, 49–51, 53, 77, 81]. In this figure, previous test results of the various hot-rolled W plates (K-doped and/or 3%Re-alloyed W) [46, 49–51, 53] and the forged round-blanks of pure W, W-1%Ta, and W-5%Ta [77] are also plotted for comparison purposes. The major fabrication conditions of the former materials were the same as those of pure W and W-Ta alloys in the present study. For the materials used in the present study, the USE and DBTT by Charpy impact test (hereinafter, $DBTT_{Charpy}$) were significantly improved by 1%Ta-alloying, whereas 3%Ta-alloying induced almost no improvement. When defining the $DBTT_{Tensile}$ by temperature dependence of TE, clear improvement of DBTT by 1%Ta-alloying and no improvement by 3%Ta-alloying were clarified for both $DBTT_{Charpy}$ and $DBTT_{Tensile}$. For 5%Ta alloying, no positive effects on DBTT were expected according to the tensile tests in the present study and Charpy impact tests by Rieth et al. [77].

As shown in Fig. 14, W-3%Ta obeyed a Hall–Petch-type relations between USE, $DBTT_{Charpy}$, and grain size (d_S), which were developed for the previously tested materials [46, 49–51, 53, 77, 81, 100–103]. In this evaluation, the USE was the average of the absorbed energies obtained by the tests at temperatures above $DBTT_{Charpy}$. The Charpy impact properties of the materials, that obeyed the Hall–Petch-type relation, could be explained by the strengthening and toughening due to grain refining. The Hall–Petch-type relation between DBTT and grain size of W materials was also reported by Bonnekoh et al. [104]. The size of cells simultaneously decreased with the size of grains (see Figs. 8 (a) and (b)). Thus, as well as the refining of grains surrounded by HAGBs, it was possible that the refining of cells might influence the strengthening and toughening. LAGBs could act as a dislocation source and thus reduce the DBTT [104]. In contrast to the aforementioned materials, the experimentally determined USE and $DBTT_{Charpy}$ of W-3%Re and K-doped W-3%Re did not agree with the values expected from the Hall–Petch-type relations. Therefore, it was indicated that the Charpy impact properties of these materials could be explained by the strengthening and toughening not only owing to grain refining but owing to other mechanisms, for instance, a solid solution strengthening and softening due to solute Re [53]. As well as these materials, higher USE and lower $DBTT_{Charpy}$ of W-1%Ta in the present study compared to the values expected from the Hall–Petch-type relation could also indicate the presence of other mechanisms in addition to grain refining.

The previous studies on the Charpy impact properties of W materials revealed that Charpy impact test specimens, in which elongated grains were aligned along the specimen length direction (e.g., along the L-S direction), did not exhibit a direct transition from brittle to ductile fractures with an increase in test temperatures and exhibited a delamination fracture between them [46, 49–51, 53, 77, 100–103]. Therefore, the DBTT of such materials was generally defined as the transition temperature from brittle to delamination fractures.

Specimens along the L-S direction made of W-Ta alloys in the present study also exhibited a brittle fracture at temperatures below $DBTT_{Charpy}$, delamination fracture at temperatures above $DBTT_{Charpy}$, and no ductile fracture up to 1000 °C. In contrast, specimens along the L-R direction made of some swaged W rods exhibited a ductile fracture even at temperatures below 1000 °C in addition to the brittle and delamination fractures [53, 77, 100–102]. Typical appearances of specimens after the Charpy impact test at temperatures above $DBTT_{Charpy}$ made of plate materials along the L-S direction are shown in Fig. 15 [46, 49–51, 53, 81]. Pure W and W-3%Ta tested at temperatures ranging from $DBTT_{Charpy}$ to 1000 °C exhibited a large area of delamination with a plastic bend deformation (see Figs. 15 (c) and (d)). The materials involving such fracture behavior exhibited relatively low USE and high $DBTT_{Charpy}$. In contrast, W-1%Ta and K-doped W-3%Re tested at temperatures ranging from $DBTT_{Charpy}$ to 1000 °C exhibited a small area of delamination with a plastic bend deformation (see Figs. 15 (a) and (b)). The materials involving such fracture behavior exhibited relatively high USE and low $DBTT_{Charpy}$. Moreover, the specimens with no notches (3 mm × 3 mm × 27 mm) made of pure W plate exhibited higher USE and similar $DBTT_{Charpy}$ compared to the specimens with a notch (4 mm × 3 mm × 27 mm, notch depth = 1 mm) (see Fig. 15 (e)). The un-notched specimens tested at temperatures above $DBTT_{Charpy}$ exhibited just a plastic bend deformation with no delamination. Thus, these results indicate that the formation and propagation of delamination made the USE lower, while induced a small influence on the $DBTT_{Charpy}$.

The fracture surface of the delamination of most W plates tested at temperatures below $DBTT_{Charpy}$ was an intergranular fracture at sub-grain boundaries [49–51, 53]. Therefore, it is possible that the plate materials exhibiting a relatively low $DBTT_{Charpy}$ like W-1%Ta and K-doped W-3%Re, which involved a small area of delamination, would have a higher strength of sub-grain boundary. Thus, controlling the sub-grain boundary strength

might be an important factor for strengthening and toughening of W materials.

3.4 Irradiation hardening

According to the previous studies regarding the recrystallized pure W and W-Ta alloys, dislocation loops were the major irradiation defect under the ion irradiation at temperatures below 800 °C [83, 86, 87]. The higher number density and smaller size of dislocation loops in the W-Ta alloys compared to pure W resulted in a higher irradiation hardening. In contrast, high temperature irradiation and post-irradiation annealing at temperatures above 800 °C induced the formation of voids in both pure W and W-Ta alloys [86, 88]. A decrease in the number density and an increase in the size of voids occurred in the W-Ta alloys with increasing temperature. Ta-alloying suppressed void formation, which was explained by a solute-vacancy trapping mechanism [86, 105]. In this temperature range, investigation of irradiation hardening has not been reported in open literature. The results of the present study of materials proton-irradiated at 1500 °C to 0.5 dpa are shown in Fig. 16. Proton irradiation induced a small irradiation hardening of specimens made of pure W and W-Ta alloys in the recrystallized condition. Irradiation hardening decreased with increasing Ta concentration. According to the aforementioned previous studies, it is possible that the reduction in irradiation hardening would be caused by the suppression of void formation, however, further microstructural studies are required to clarify this.

In contrast to the irradiation response of the recrystallized specimens, specimens made of pure W and W-Ta alloys in the as-received condition exhibited a reduction in Vickers hardness by proton irradiation compared to the non-irradiated state. The absolute value of hardness reduction in as-received materials was higher than the value of hardness increment (irradiation hardening) of recrystallized materials. For the pure W in the as-received condition, voids were observed as irradiation-induced defects, whose diameter was in the range of 3–5

nm, as well as the previous studies on recrystallized materials (see TEM image in Fig. 16). Moreover, no dislocations and cell structures were observed, which could indicate that the microstructure (dislocations and cells, etc.) formed during material fabrication were tended to disappear during the proton irradiation at 1500 °C. This microstructural change could be attributed to the microstructural recovery followed by recrystallization during irradiation. Because a relatively slight increase in hardness due to void formation and a relatively significant decrease in hardness by recovery and recrystallization occurred simultaneously, a relatively significant hardness reduction could occur in the as-received pure W after proton irradiation. In contrast to the pure W, W-5%Ta in the as-received condition exhibited no visible irradiation defects, no dislocations and cell structures, and a relatively slight reduction in hardness. Suppression of void formation might occur owing to 5%Ta-alloying. Because the recrystallization temperature of W-5%Ta was higher than that of pure W (see Fig. 7), the recovery and recrystallization of W-5%Ta during proton irradiation could not be advanced compared to pure W. Therefore, reduction in hardness during proton irradiation was smaller for W-5%Ta than for pure W. As mentioned before, Ta concentrations ranging from 1 to 5% induced small differences in recrystallization temperature. In contrast, the hardness reduction owing to microstructural recovery was more significant, when the Ta concentration was low (see Fig. 7). Therefore, the decrease in the hardness reduction with increasing Ta concentration could be owing to not only the difference in resistance to recrystallization but also the difference in resistance to microstructural recovery. Based on these experimental results, one of the major factors determining the hardness change of as-received materials by proton irradiation at 1500 °C could be recovery and recrystallization during irradiation. To clarify whether the hardness reduction was either due to irradiation or recrystallization, or due to both of them, rather detailed TEM observations are required in addition to hardness measurements.

As well as the W-3%Ta in the as-received condition, hardening reduction occurred in W-3%Re in the as-received condition, which was larger than that of W-3%Ta. If recovery and recrystallization were the major factors determining the hardness change of as-received materials by proton irradiation at 1500 °C, difference in the hardness reduction between W-3%Ta and W-3%Re would be attributed to the difference in resistance to recrystallization. The recrystallization temperature of W-3%Re through isochronal annealing for 1 h was 1500 °C [50]. However, the microstructure evolution of W by irradiation could be significantly changed by Re-alloying, for instance, void formation by irradiation below 0.5 dpa was suppressed by the solute Re [53, 58, 61, 62, 64–66]. Thus, further microstructural study is planned to clarify the effects of Ta and Re at a higher temperature range above 1000 °C.

According to the present study, the formation and growth of irradiation defects accompanied by thermally induced microstructural recovery and recrystallization should be simultaneously considered under high temperature irradiation (e.g., above 1000 °C) of W materials in the as-received condition. Below a certain level of displacement damage (e.g., below 0.5 dpa), it is possible that the hardness change of materials in the as-received condition during irradiation could be dominated by recovery and recrystallization rather than irradiation defects. In contrast, above a certain level of displacement damage, it is possible that the behavior of the hardness change of materials in the as-received condition during irradiation would be close to that of the material in the recrystallized condition because the change in microstructure owing to recrystallization could be saturated. Subsequently, the irradiation defects could accumulate in the recrystallized microstructure. Advanced W materials such as W-Ta and W-Re alloys could exhibit improved recrystallization resistance compared to pure W. Thus, the behavior of irradiation hardening is important for these materials during a period in which thermally induced recovery and recrystallization cannot be

negligible.

3.5 Validity of Ta alloying for fusion reactor applications

The present study revealed that W-Ta alloys (Ta: 1–5%) could be promising for fusion reactor applications from the perspective of fundamental mechanical properties and resistance to recrystallization in the non-irradiated state. In particular, W-1%Ta alloy exhibited superior ductility (TE, RA, USE, and DBTT) compared with the other alloys. The recrystallization temperature and DBTT could be factors in determining the available temperature range of the actual components of the fusion reactors. Thus, as shown in Fig. 17, temperature range from DBTT ($DBTT_{Tensile}$ and $DBTT_{Charpy}$) to the recrystallization temperature by isochronal annealing for 1 h (T_{Rec}) in the non-irradiated state was compared among hot-rolled W plates made of pure W, W-Ta alloys, and K-doped and/or Re-alloyed W [53]. It was clarified that W-1%Ta could be competitive, even in this integrated evaluation.

For the Charpy impact properties, hot-rolled W-Ta alloy plates in the present study exhibited better performance compared to the forged round-blank W-Ta alloys in the previous study, regardless of the Ta concentration [77]. This might be caused by the condition of the raw material (e.g., W powder) and ingot, the microstructure controlled by the fabrication processes, and the impurities introduced during fabrication. The details are not certain, however, in any cases, it is not appropriate to discuss the goodness of a material based on its major chemical composition alone.

The material performance required for the actual components of fusion reactors has also been studied in the framework of our research. As well as the fundamental mechanical properties in the non-irradiated state, several studies have indicated the promising feasibility of W-Ta alloys.

Considering the utilization of the material for high-temperature components of

fusion reactors, thermal properties are very important. In general, the thermal conductivity of alloyed materials is lower than that of pure material. Therefore, degradation of the thermal conductivity caused by Ta-alloying was concerned before the present study. As part of the evaluation of thermal properties, the thermal diffusivity of W-Ta alloys in the as-received condition was measured and compared with that of pure W and W-Re alloys in the previous studies (see Fig. 18) [44, 47]. Although the thermal diffusivity of W-Ta alloys was lower than that of pure W, the reduction ratio was not higher than that of W-Re alloys with the same concentration of alloying elements. Moreover, the operation temperature of high-temperature component of fusion reactors is higher than the coolant temperature (e.g., approximately 300 °C for water-cooled devises). Because the thermal conductivity and diffusivity of alloyed materials grew close to those of pure material with increasing temperature, the negative effects of alloying could be small if high temperature operation is considered.

As well as the thermal properties, the resistance against high heat flux exposure expected in the plasma-facing materials of fusion reactor components should be considered. As part of the evaluation of the resistance against high heat flux exposure, thermal shock tests of pure W and W-3%Ta were performed [81]. These materials were the same as those used in the present study. In this experiment, a linear plasma device, PSI-2, at Forschungszentrum Jülich was used. Simultaneous exposure of a pulsed Nd:YAG laser and steady state deuterium (D) plasma was applied under the following conditions; base temperature, number of laser pulses, laser power density, and D-plasma fluence were 700 °C, 10^3–10^5, 0.38 GW/m^2, and 10^{24}–10^{25} m^{-2}, respectively. D-plasma exposure was applied to investigate the effect of the high chemical affinity of Ta with hydrogen and hydrogen-induced embrittlement of Ta. Fig. 19 shows the surface images and surface roughness values after the thermal shock tests under the most severe condition. Surface degradation of W-3%Ta was suppressed compared to that of pure W regardless of the test conditions. Although it was concerned that the effect of

D-plasma exposure might be much more pronounced in the W-Ta alloy, the present study revealed no clear negative effects.

Advanced W materials such as the W-Ta alloy proposed in the present study would be mostly applied to the DEMO reactor and beyond. For such applications, the neutron irradiation response is a key factor in the structural strength and life of the components. The present study indicated that the effect of thermally induced microstructural recovery and recrystallization is an important factor for understanding the time history of the evolution of irradiation hardening. According to the present study, W-Ta alloys exhibited no negative response to proton irradiation compared with pure and Re-alloyed W materials. Moreover, according to the previous studies [82, 84, 85], the Re-clustering in the W-Re-Ta ternary alloy was suppressed compared to that in the W-Re binary alloy, which resulted in suppressed irradiation hardening owing to cluster formation. The solid transmutation reaction could produce Re in W, and thereafter, the formation of Re-clusters and precipitates could occur, resulting in enhanced irradiation hardening in addition to hardening owing to displacement damage [58–73]. Thus, the application of Ta-alloying to W materials could be promising from the perspective of improving the long-term irradiation resistance accompanied by solid transmutation, as well as the thermo-mechanical properties in the non-irradiated state. However, the irradiation conditions adopted in the present study were limited. Therefore, it might be difficult to comment about the performance of the material under fusion irradiation conditions. Consequently, further irradiation studies are required to clarify the validity of Ta alloying for fusion reactor applications.

4. Conclusion

W plates alloyed by 1–5%Ta were developed to investigate the availability of W-Ta binary alloy system for fusion reactor applications. In addition to the mechanical properties

and recrystallization resistance, the following material performances required in actual fusion reactors were studied in the framework of this research; thermal properties, resistance against high heat flux exposure, and irradiation response. Through this study, W-Ta alloys were demonstrated to be promising for fusion reactor applications. The individual investigation results are summarized as follows:

(1) Ta-alloying induced a refining of grains and cells, however, Ta concentrations ranging from 1 to 5% made no significant difference.

(2) Grain refining and solute Ta increased the resistance to recrystallization and improved strength. For ductility and toughness, W-3%Ta and W-5%Ta alloys exhibited no improvement compared to pure W, whereas W-1%Ta alloy exhibited superior ductility, including DBTT, which might be related to the improved strength of sub-grain boundary.

(3) Proton irradiation study was performed at 1500 °C to 0.5 dpa. For the materials in the recrystallized condition, the irradiation hardening (increase in hardness) decreased with an increase in Ta concentration. In contrast, the materials in the as-received condition exhibited a reduction in hardness. The hardness reduction decreased with an increase in Ta concentration. One of the major factors determining the hardness change of the as-received materials at such high temperature irradiation could be a microstructural recovery followed by recrystallization.

(4) For the thermal properties important for high-temperature components of fusion reactors, the reduction ratio of thermal diffusivity by Ta-alloying was lower than that of Re-alloying when the concentration of the alloying element was the same.

(5) For the resistance against high heat flux exposure expected in the fusion reactor components, the degradation of W-3%Ta was suppressed compared to pure W after thermal shock tests by simultaneous exposure of pulsed laser and steady state D-plasma.

Although it was concerned that the effect of D-plasma exposure might be much more pronounced in the W-Ta alloy, the present study revealed no clear negative effects.

CRediT author statement

Shuhei Nogami	Management, Experiments, Data analysis
Itsuki Ozawa	Experiments, Data analysis
Daisuke Asami	Experiments, Data analysis
Naoya Matsuta	Experiments, Data analysis
Seiji Nakabayashi	Data analysis
Siegfried Baumgärtner	Experiments
Philipp Lied	Experiments
Kiyohiro Yabuuchi	Experiments
Takeshi Miyazawa	Experiments
Yuta Kikuchi	Experiments
Marius Wirtz	Experiments, Data analysis
Michael Rieth	Data analysis
Akira Hasegawa	Data analysis

Declaration of interests

☒ The authors declare that they have no known competing financial interests or personal relationships that could have appeared to influence the work reported in this paper.

Acknowledgements

This work was performed with the support and under the auspices of the NIFS Collaboration Research program (NIFS19HDAF002). TEM observation was supported by the Joint Usage/Research Program on Zero-Emission Energy Research, Institute of Advanced Energy, Kyoto University (ZE2020A-11). Measurement of thermal diffusivity was performed under the GIMRT Program of the Institute for Materials Research, Tohoku University (Proposal No. 202012-RDKGE-0204). Authors are grateful to Prof. R. Kasada and H. You for their support to our thermal diffusivity measurement. Authors are grateful to Mr. S. Fujiwara of Dai-Ichi Kiden Co., Ltd. for his support to our heat treatment, and to Dr. S. Matsuyama and Ms. M. Miwa for their support to our ion irradiation experiment using the Dynamitron accelerator.

References

[1] P. Gumbsch, Brittle fracture and the brittle-to-ductile transition of tungsten, J. Nucl. Mater. **323** (2003) 304–312.

[2] M. Faleschini, H. Kreuzer, D. Kiener, R. Pippan, Fracture toughness investigations of tungsten alloys and SPD tungsten alloys, J. Nucl. Mater. **367–370** (2007) 800–805.

[3] A. Giannattasio, M. Tanaka, T. D. Joseph, S. G. Roberts, An empirical correlation between temperature and activation energy for brittle-to-ductile transitions in single-phase materials, Phys. Scr. **T128** (2007) 87–90.

[4] A. Giannattasio, S. G. Roberts, Strain-rate dependence of the brittle-to-ductile transition temperature in tungsten, Phil. Mag. **87 (17)** (2007) 2589–2598.

[5] D. Rupp, S. M. Weygand, Experimental investigation of the fracture toughness of polycrystalline tungsten in the brittle and semi-brittle regime, J. Nucl. Mater. **386–388** (2009) 591–593.

[6] D. Rupp, R. Mönig, P. Gruber, S. M. Weygand, Fracture toughness and microstructural characterization of polycrystalline rolled tungsten, Int. J. Refract. Met. Hard Mater. **28** (2010) 669–673.

[7] D. Rupp, S. M. Weygand, Anisotropic fracture behaviour and brittle to ductile transition of polycrystalline tungsten, Phil. Mag. **90 (30**) (2010) 4055–4069.

[8] D. Rupp, S. M. Weygand, Loading rate dependence of the fracture toughness of polycrystalline tungsten, J. Nucl. Mater. **417** (2011) 477–480.

[9] E. Gaganidze, D. Rupp, J. Aktaa, Fracture behaviour of polycrystalline tungsten, J. Nucl. Mater. **446** (2014) 240–245.

[10] A. V. Babak, Evaluating the crack resistance of tungsten at high temperatures, Strength Mater. **14** (1982) 1389–1391.

[11] N. D. Bega, A. V. Babak, E. I. Uskov, Recrystallization and embrittlement of sintered

tungsten, Soviet Powder Metall. Met. Ceram. **21** (1982) 408–411.

[12] A. V. Babak, Effect of recrystallization on the fracture toughness of tungsten, Soviet Powder Metall. Met. Ceram. **22** (1983) 316–318.

[13] A. V. Babak, E. I. Uskov, High-temperature embrittlement of tungsten, Strength Mater. **15** (1983) 667–672.

[14] R. C. Rau, J. Moteff, R. L. Ladd, Comparison of microstructure with mechanical properties of irradiated tungsten, J. Nucl. Mater. **24** (1967) 164–173.

[15] I. V. Gorynin, V. A. Ignatov, V. V. Rybin, S. A. Fabritsiev, V. A. Kazakov, V. P. Chakin, V. A. Tsykanov, V. R. Barabash, Y. G. Prokofyev, Effects of neutron irradiation on properties of refractory metals, J. Nucl. Mater. **191–194** (1992) 421–425.

[16] J. M. Steichen, Tensile properties of neutron irradiated TZM and tungsten, J. Nucl. Mater. **61** (1976) 13–19.

[17] P. Krautwasser, H. Derz, E. Kny, Influence of fast neutron fluence on the DBTT of W, W10Re, and W3.4Ni1.6Fe, in: Proceedings of the 12th International PLANSEE Seminar, 1989, pp. 673–681.

[18] K. Farrell, A. C. Schaffhauser, J. O. Stiegler, Recrystallization, grain growth and the ductile-brittle transition in tungsten sheet, J. Less-Common Met. **13** (1967) 141–155.

[19] Q. Wei, L. J. Kecskes, Effect of low-temperature rolling on the tensile behavior of commercially pure tungsten, Mater. Sci. Eng. A **491** (2008) 62–69.

[20] A. Luo, D. L. Jacobson, K. S. Shin, Solution softening mechanism of iridium and rhenium in tungsten at room temperature, Int. J. Refract. Met. Hard Mater. **10** (1991) 107–114.

[21] P. Makarov, K. Povarova, Development of tungsten-based vacuum melted and powder structural alloys, Int. J. Refract. Met. Hard Mater. **20** (2002) 277–285.

[22] P. Schade, 100 years of doped tungsten wire, Int. J. Refract. Met. H **28** (2010) 648–660.

[23] G. Geach, J. Hughes, The alloys of rhenium with molybdenum or with tungsten and having good high temperature properties, in: Proceedings of the 2nd International PLANSEE Seminar, 1955, pp. 245–253.

[24] H. Li, S. Wurster, C. Motz, L. Romaner, C. Ambrosch-Draxl, R. Pippan, Dislocation-core symmetry and slip planes in tungsten alloys: Ab initio calculations and microcantilever bending experiments, Acta Mater. **60** (2012) 748–758.

[25] L. Romaner, C. Ambrosch-Draxl, R. Pippan, Effect of rhenium on the dislocation core structure in tungsten, Phys. Rev. Lett. **104 (19)** (2010) 195503.

[26] K. Shin, A. Luo, B. Chen, D. Jacobson, High-temperature properties of particle-strengthened W-Re, JOM **42** (1990) 12–15.

[27] T. Leonhardt, Properties of tungsten-rhenium and tungsten-rhenium with hafnium carbide, JOM **61** (2009) 68–71.

[28] Z. Xie, R. Liu, T. Zhang, Q. Fang, C. Liu, X. Liu, G. Luo, Achieving high strength/ductility in bulk W-Zr-Y_2O_3 alloy plate with hybrid microstructure, Mater. Des. **107** (2016) 144–152.

[29] M. Mabuchi, K. Okamoto, N. Saito, M. Nakanishi, Y. Yamada, T. Asahina, Tensile properties at elevated temperature of W-1%La_2O_3, Mater. Sci. Eng. A **214** (1996) 174–176.

[30] M. Mabuchi, K. Okamoto, N. Saito, T. Asahina, T. Igarashi, Deformation behavior and strengthening mechanisms at intermediate temperatures in W-1%La_2O_3, Mater. Sci. Eng. A **237** (1997) 241–249.

[31] H. Kurishita, S. Matsuo, H. Arakawa, T. Sakamoto, S. Kobayashi, K. Nakai, T. Takida, M. Kato, M. Kawai, N. Yoshida, Development of re-crystallized W–1.1%TiC with enhanced room-temperature ductility and radiation performance, J. Nucl. Mater. **398** (2010) 87–92.

[32] M. Kawai, H. Kurishita, H. Kokawa, S. Watanabe, N. Sakaguchi, K. Kikuchi, S. Saito, T. Yoshiie, H. Iwase, T. Ito, S. Hashimoto, Y. Kaneko, M. Futakawa, S. Ishino, Development of advanced materials for spallation neutron sources and radiation damage simulation based on multi-scale models, J. Nucl. Mater. **431** (2012) 16–25.

[33] S. Miao, Z. Xie, X. Yang, R. Liu, R. Gao, T. Zhang, X. Wang, Q. Fang, C. Liu, G. Luo, X. Liu, Y. Lian, Effect of hot rolling and annealing on the mechanical properties and thermal conductivity of W-0.5 wt.% TaC alloys, Int. J. Refract. Met. Hard Mater. **56** (2016) 8–17.

[34] Z. Xie, R. Liu, S. Miao, X. Yang, T. Zhang, X. Wang, Q. Fang, C. Liu, G. Luo, Y. Lian, X. Liu, Extraordinary high ductility/strength of the interface designed bulk W-ZrC alloy plate at relatively low temperature, Sci. Rep. **5** (2015) 16014.

[35] J. W. Pugh, On the short time creep rupture properties of lamp wire, Metall. Trans. A **4** (1973) 533–538.

[36] P. K. Wright, The high temperature creep behavior of doped tungsten wire, Metall. Trans. A **9** (1978) 955–963.

[37] D. B. Snow, The recrystallization of commercially pure and doped tungsten wire drawn to high strain, Metall. Trans. A **10** (1979) 815–821.

[38] M. Fukuda, S. Nogami, K. Yabuuchi, A. Hasegawa, T. Muroga, Anisotropy in the mechanical properties of potassium and rhenium doped tungsten alloy plates for fusion reactor applications, Fus. Sci. Technol. **68** (2015) 690–693.

[39] K. Sasaki, K. Yabuuchi, S. Nogami, A. Hasegawa, Effects of temperature and strain rate on the tensile properties of potassium-doped tungsten, J. Nucl. Mater. **461** (2015) 357–364.

[40] S. Nogami, W. H. Guan, M. Fukuda, A. Hasegawa, Effect of microstructural anisotropy on the mechanical properties of K-doped tungsten rods for plasma facing components,

Fus. Eng. Des. **109–111** (2016) 1549–1553.

[41] W. H. Guan, S. Nogami, M. Fukuda, A. Hasegawa, Tensile and fatigue properties of potassium doped and rhenium containing tungsten rods for fusion reactor applications, Fus. Eng. Des. **109–111** (2016) 1538–1542.

[42] M. Fukuda, S. Nogami, W. H. Guan, A. Hasegawa, T. Muroga, Analysis of the temperature and thermal stress in pure tungsten monoblock during heat loading and the influences of alloying and dispersion strengthening on these responses, Fus. Eng. Des. **107** (2016) 44–50.

[43] M. Fukuda, T. Tabata, A. Hasegawa, S. Nogami, T. Muroga, Strain rate dependence of tensile properties of tungsten alloys for plasma-facing components in fusion reactors, Fus. Eng. Des. **109–111** (2016) 1674–1677.

[44] S. Nogami, W. H. Guan, A. Hasegawa, M. Fukuda, Feasibility of utilizing tungsten rod for fusion reactor divertor, Fus. Sci. Technol. **72** (2017) 673–679.

[45] S. Nogami, W. H. Guan, T. Hattori, K. James, A. Hasegawa, Improved structural strength and lifetime of monoblock divertor targets by using doped tungsten alloys under cyclic high heat flux loading, Phys. Scr. **T170** (2017) 014011.

[46] S. Nogami, S. Watanabe, J. Reiser, M. Rieth, S. Sickinger, A. Hasegawa, A review of impact properties of tungsten materials, Fus. Eng. Des. **135** (2018) 196–203.

[47] M. Fukuda, A. Hasegawa, S. Nogami, Thermal properties of pure tungsten and its alloys for fusion applications, Fus. Eng. Des. **132** (2018) 1–6.

[48] S. Nogami, H. Noto, M. Toyota, T. Hattori, K. Otomo, A. Hasegawa, Solid state diffusion bonding of doped tungsten alloys with different thermo-mechanical properties, Fus. Eng. Des. **136** (2018) 76–81.

[49] S. Nogami, S. Watanabe, J. Reiser, M. Rieth, S. Sickinger, A. Hasegawa, Improvement of impact properties of tungsten by potassium doping, Fus. Eng. Des. **140** (2019) 48–61.

[50] S. Watanabe, S. Nogami, J. Reiser, M. Rieth, S. Sickinger, S. Baumgärtner, T. Miyazawa, A. Hasegawa, Tensile and impact properties of tungsten-rhenium alloy for plasma-facing components in fusion reactor, Fus. Eng. Des. **148** (2019) 111323.

[51] S. Nogami, A. Hasegawa, M. Fukuda, S. Watanabe, J. Reiser, M. Rieth, Tungsten modified by potassium doping and rhenium addition for fusion reactor applications, Fus. Eng. Des. **152** (2020) 111445.

[52] S. Nogami, G. Pintsuk, K. Matsui, S. Watanabe, M. Wirtz, T. Loewenhoff, A. Hasegawa, Thermal shock behavior of potassium doped and rhenium added tungsten alloys, Phys. Scr. **T171** (2020) 014020.

[53] S. Nogami, A. Hasegawa, M. Fukuda, M. Rieth, J. Reiser, G. Pintsuk, Mechanical properties of tungsten: Recent research on modified tungsten materials in Japan, J. Nucl. Mater. **543** (2021) 152506.

[54] C. Yin, D. Terentyev, T. Zhang, S. Nogami, S. Antusch, C. Chang, R. H. Petrov, T. Pardoen, Ductile to brittle transition temperature of advanced tungsten alloys for nuclear fusion applications deduced by miniaturized three-point bending tests, Int. J. Refract. Met. Hard Mater. **95** (2021) 105464.

[55] T. Miyazawa, L. M. Garrison, J. W. Geringer, M. Fukuda, Y. Katoh, T. Hinoki, A. Hasegawa, Neutron irradiation effects on the mechanical properties of powder metallurgical processed tungsten alloys, J. Nucl. Mater. **529** (2020) 151910.

[56] T. Miyazawa, L. M. Garrison, J. W. Geringer, J. R. Echols, M. Fukuda, Y. Katoh, T. Hinoki, A. Hasegawa, Tensile properties of powder-metallurgical-processed tungsten alloys after neutron irradiation near recrystallization temperatures, J. Nucl. Mater. **542** (2020) 152505.

[57] S. Nogami, D. Terentyev, A. Zinovev, C. Yin, M. Rieth, G. Pintsuk, A. Hasegawa, Neutron irradiation tolerance of potassium-doped and rhenium-alloyed tungsten, J. Nucl.

Mater. **553** (2021) 153009.

[58] M. Fukuda, T. Tanno, S. Nogami, A. Hasegawa, Effects of Re content and fabrication process on microstructural changes and hardening in neutron irradiated tungsten, Mater. Trans. **53** (2012) 2145–2150.

[59] M. Fukuda, K. Yabuuchi, S. Nogami, A. Hasegawa, T. Tanaka, Microstructural development of tungsten and tungsten–rhenium alloys due to neutron irradiation in HFIR, J. Nucl. Mater. **455** (2014) 460–463.

[60] M. Fukuda, N. A. P. Kiran Kumar, T. Koyanagi, L. M. Garrison, L. L. Snead, Y. Katoh, A. Hasegawa, Neutron energy spectrum influence on irradiation hardening and microstructural development of tungsten, J. Nucl. Mater. **479** (2016) 249–254.

[61] T. Tanno, A. Hasegawa, J. -C. He, M. Fujiwara, S. Nogami, M. Satou, T. Shishido, K. Abe, Effects of transmutation elements on neutron irradiation hardening of tungsten, Mater. Trans. **48-9** (2007) 2399–2402.

[62] T. Tanno, A. Hasegawa, M. Fujiwara, J. -C. He, S. Nogami, M. Satou, T. Shishido, K. Abe, Precipitation of solid transmutation elements in irradiated tungsten alloys, Mater. Trans. **49-10** (2008) 2259–2264.

[63] T. Tanno, A. Hasegawa, J. -C. He, M. Fujiwara, M. Satou, S. Nogami, K. Abe, T. Shishido, Effects of transmutation elements on the microstructural evolution and electrical resistivity of neutron-irradiated tungsten, J. Nucl. Mater. **386–388** (2009) 218–221.

[64] A. Hasegawa, T. Tanno, S. Nogami, M. Satou, Property change mechanism in tungsten under neutron irradiation in various reactors, J. Nucl. Mater. **417** (2011) 491–494.

[65] A. Hasegawa, M. Fukuda, S. Nogami, K. Yabuuchi, Neutron irradiation effects on tungsten materials, Fus. Eng. Des. **89** (2014) 1568–1572.

[66] A. Hasegawa, M. Fukuda, K. Yabuuchi, S. Nogami, Neutron irradiation effects on the

microstructural development of tungsten and tungsten alloys, J. Nucl. Mater. **471** (2016) 175–183.

[67] T. Hwang, A. Hasegawa, K. Tomura, N. Ebisawa, T. Toyama, Y. Nagai, M. Fukuda, T. Miyazawa, T. Tanaka, S. Nogami, Effect of neutron irradiation on rhenium cluster formation in tungsten and tungsten-rhenium alloys, J. Nucl. Mater. **507** (2018) 78–86.

[68] Y. Katoh, L. L. Snead, L. M. Garrison, X. Hu, T. Koyanagi, C. M. Parish, P. D. Edmondson, M. Fukuda, T. Hwang, T. Tanaka, A. Hasegawa, Response of un- alloyed tungsten to mixed spectrum neutrons, J. Nucl. Mater. **520** (2019) 193–207.

[69] X. Hu, T. Koyanagi, M. Fukuda, Y. Katoh, L. L. Snead, B. D. Wirth, Defect evolution in single crystalline tungsten following low temperature and low dose neutron irradiation, J. Nucl. Mater. **470** (2016) 278–289.

[70] X. Hu, T. Koyanagi, M. Fukuda, N. A. P. Kiran Kumar, L. L. Snead, B. D. Wirth, Y. Katoh, Irradiation hardening of pure tungsten exposed to neutron irradiation, J. Nucl. Mater. **480** (2016) 235–243.

[71] X. Hu, C. M. Parish, K. Wang, T. Koyanagi, B. P. Eftink, Y. Katoh, Transmutation-induced precipitation in tungsten irradiated with a mixed energy neutron spectrum, Acta Mater. **165** (2019) 51–61.

[72] T. Koyanagi, N. A. P. Kiran Kumar, T. Hwang, L. M. Garrison, X. Hu, L. L. Snead, Y. Katoh, Microstructural evolution of pure tungsten neutron irradiated with a mixed energy spectrum, J. Nucl. Mater. **490** (2017) 66–74.

[73] M. Klimenkov, U. Jäntsch, M. Rieth, H. C. Schneider, D. E. J. Armstrong, J. Gibson, S. G. Roberts, Effect of neutron irradiation on the microstructure of tungsten, Nucl. Mater. Energy **9** (2016) 480–483.

[74] H. Okamoto, M. Schlesinger, E. Mueller, ASM Handbook Volume 3, Alloy phase diagrams, ASM International, (2016).

[75] T. Noda, F. Abe, H. Araki, M. Okada, Materials selection for reduced activation of fusion reactors, J. Nucl. Mater. **155–157** (1988) 581–584.

[76] P. J. Maziasz, R. L. Klueh, Precipitation sensitivity to alloy composition in Fe-Cr-Mn austenitic steels developed for reduced activation for fusion application, ASTM STP **1047** (1990) 56–79.

[77] M. Rieth, J. Reiser, B. Dafferner, S. Baumgärtner, The impact of refractory material properties on the helium cooled divertor design, Fusion Sci. Technol. **61** (2012) 381–384.

[78] S. Wurster, B. Gludovatz, A. Hoffmann, R. Pippan, Fracture behaviour of tungsten–vanadium and tungsten–tantalum alloys and composites, J. Nucl. Mater. **413** (2011) 166–176.

[79] K. Schmid, V. Rieger, A. Manhard, Comparison of hydrogen retention in W and W/Ta alloys, J. Nucl. Mater. **426** (2012) 247–253.

[80] Ch. Linsmeier, M. Rieth, J. Aktaa, T. Chikada, A. Hoffmann, J. Hoffmann, A. Houben, H. Kurishita, X. Jin, M. Li, A. Litnovsky, S. Matsuo, A. von Müller, V. Nikolic, T. Palacios, R. Pippan, D. Qu, J. Reiser, J. Riesch, T. Shikama, R. Stieglitz, T. Weber, S. Wurster, J.-H. You, Z. Zhou, Development of advanced high heat flux and plasma-facing materials, Nucl. Fusion **57** (2017) 092007.

[81] S. Nogami, M. Wirtz, P. Lied, T. Chikada, Thermal shock behavior under deuterium plasma exposure of tungsten–tantalum alloys, Phys. Scr. **96** (2021) 114011.

[82] A. Xu, D. E. J. Armstrong, C. Beck, M. P. Moody, G. D. W. Smith, P. A. J. Bagot, S. G. Roberts, Ion-irradiation induced clustering in W-Re-Ta, W-Re and W-Ta alloys: An atom probe tomography and nanoindentation study, Acta Mater. **124** (2017) 71–78.

[83] X. Yi, Michael L. Jenkins, K. Hattar, P. D. Edmondson, S. G. Roberts, Characterisation of radiation damage in W and W-based alloys from 2 MeV self-ion near-bulk implantations, Acta Mater. **92** (2015) 163–177.

[84] D. E. J. Armstrong, A. J. Wilkinson, S. G. Roberts, Mechanical properties of ion-implanted tungsten–5 wt% tantalum, Phys. Scr. **T145** (2011) 014076.

[85] D. E. J. Armstrong, X. Yi, E. A. Marquis, S. G. Roberts, Hardening of self ion implanted tungsten and tungsten 5-wt% rhenium, J. Nucl. Mater. **432** (2013) 428–436.

[86] I. Ipatova, R. W. Harrison, D. Terentyev, S. E. Donnelly, E. Jimenez-Melero, Thermal evolution of the proton irradiated structure in tungsten-5 wt% tantalum, J. Fus. Energ. **36** (2017) 234–239.

[87] I. Ipatova, R. W. Harrison, P. T. Wady, S. M. Shubeita, D. Terentyev, S. E. Donnelly, E. Jimenez-Melero, Structural defect accumulation in tungsten and tungsten-5wt.% tantalum under incremental proton damage, J. Nucl. Mater. **501** (2018) 329–335.

[88] I. Ipatova, R. W. Harrison, S. E. Donnelly, M. J. D. Rushton, S. C. Middleburgh, E. Jimenez-Melero, Void evolution in tungsten and tungsten-5wt.% tantalum under in-situ proton irradiation at 800 and 1000 °C, J. Nucl. Mater. **526** (2019) 151730.

[89] I. Ipatova, G. Greaves, S. Pacheco-Gutiérrez, S. C. Middleburgh, M. J. D. Rushton, E. Jimenez-Melero, In-situ TEM investigation of nano-scale helium bubble evolution in tantalum-doped tungsten at 800°C, J. Nucl. Mater. **550** (2021) 152910.

[90] ASTM E112–13, Standard methods for determining the average grain size, Annual Book of ASTM, 2013.

[91] DIN EN ISO 14556:2017-05, Metallische Werkstoffe - Kerbschlagbiegeversuch nach Charpy (V-Kerb) - Instrumentiertes Prüfverfahren (ISO 14556:2015); Deutsche Fassung EN ISO 14556:2015 [in German].

[92] J. F. Ziegler, J. P. Biersack, The stopping and range of ions in matter, Treatise on Heavy-Ion Science, 1985, 93–129.

[93] ASTM E521-96, Standard practice for neutron radiation damage simulation by charged-particle irradiation, Annual Book of ASTM, 1996.

[94] R. D. Cowan, Pulse method of measuring thermal diffusivity at high temperatures, J. App. Phys. **34** (1963) 926–927.

[95] L. Vegard, Die konstitution der mischkristalle und die raumfüllung der atome, Z. Phys. **5** (1921) 17–26.

[96] Y. Mutoh, K. Ichikawa, K. Nagata, M. Takeuchi, Effect of rhenium addition on fracture toughness of tungsten at elevated temperatures, J. Mater. Sci. **30** (1995) 770–775.

[97] B. Gludovatz, S. Wurster, A. Hoffmann, R. Pippan, Fracture toughness of poly-crystalline tungsten alloys, Int. J. Refract. Met. Hard Mater. **28** (2010) 674–678.

[98] M. Fukuda, S. Nogami, A. Hasegawa, H. Usami, K. Yabuuchi, T. Muroga, Tensile properties of K-doped W–3%Re, Fus. Eng. Des. **89** (2014) 1033–1036.

[99] M. F. Ashby, A first report on deformation-mechanism maps, Acta Metall. **20** (1972) 887–897.

[100] M. Rieth, D. Armstrong, B. Dafferner, S. Heger, A. Hoffmann, M.-D. Hoffmann, U. Jäntsch, C. Kübel, E. Materna-Morris, J. Reiser, M. Rohde, T. Scherer, V. Widak, H. Zimmermann, Tungsten as a structural divertor material, Advances in Science and Technology **73** (2010) 11–21.

[101] M. Rieth, A. Hoffmann, Impact bending tests on selected refractory materials, Advances in Science and Technology **59** (2008) 101–104.

[102] M. Rieth, A. Hoffmann, Influence of microstructure and notch fabrication on impact bending properties of tungsten materials, Int. J. Refract. Met. Hard Mater. **28** (2010) 679–686.

[103] J. Reiser, M. Rieth, B. Dafferner, A. Hoffmann, Charpy impact properties of pure tungsten plate material in as-received and recrystallized condition (1 h at 2000 °C (2273 K)), J. Nucl. Mater. **442** (2013) S204–S207.

[104] C. Bonnekoh, A. Hoffmann, J. Reiser, The brittle-to-ductile transition in cold rolled

tungsten: On the decrease of the brittle-to-ductile transition by 600 K to −65 °C, Int. J. Refract. Met. Hard Mater. **71** (2018) 181–189.

[105] F. A. Smidt, J. A. Sprague, Suppression of void nucleation by a vacancy trapping mechanism, Scr. Metall. **7** (1973) 495–502.

[106]

Table 1 Concentrations of Ta and interstitial impurity atoms (C, O, and N) in pure W, W-1%Ta, W-3%Ta, W-5%Ta, and W-3%Re plates.

Material	C [ppm]	O [ppm]	N [ppm]	Ta [mass %]
Pure W	<10	<10	<10	–
W-1%Ta	<10	20	<10	0.96
W-3%Ta	<10	10	<10	3.0
W-5%Ta	<10	20	<10	5.0
W-3%Re	<10	<10	<10	–

Fig. 1 (a) Definitions of directions of materials and specimens (L, T, S, and L-S direction), and drawings of (b) tensile and (c) Charpy impact test specimens.

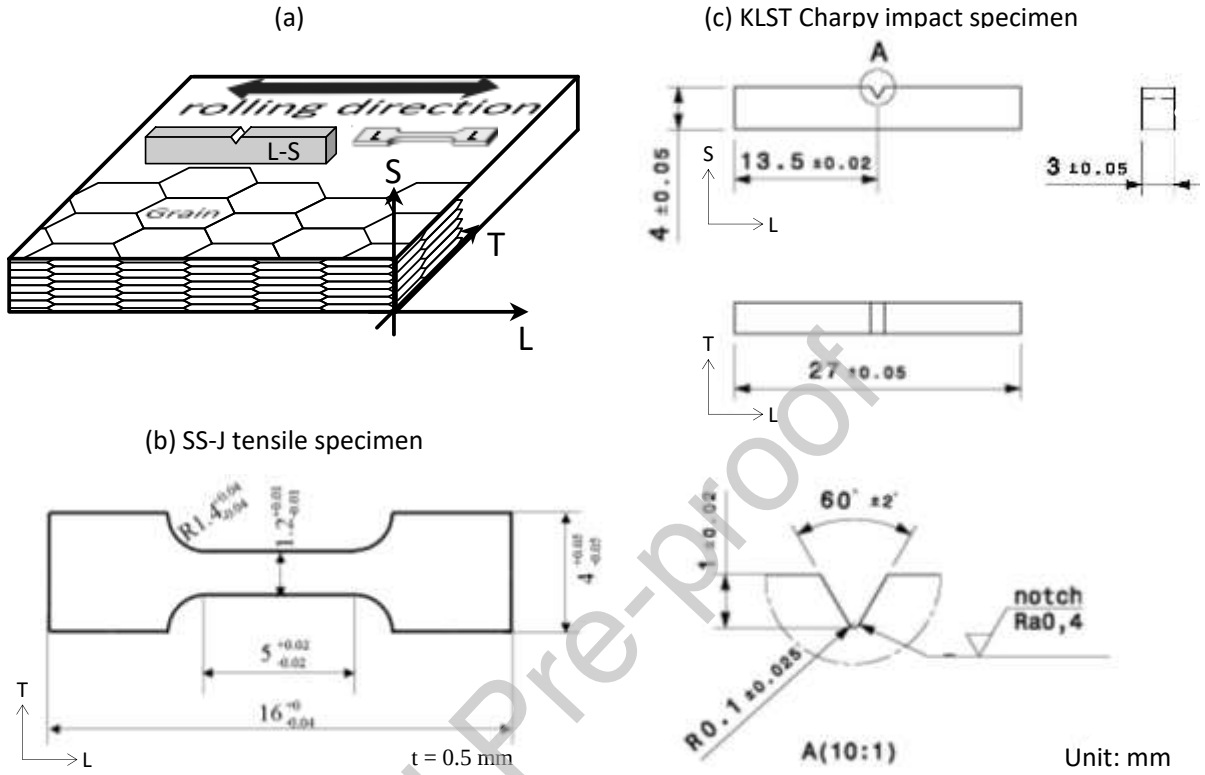

Fig. 2 Distribution of displacement damage in W-5%Ta after 3 MeV proton irradiation calculated using SRIM-2013 [92]. Threshold displacement energies of W and Ta was were assumed to be 90 eV [93].

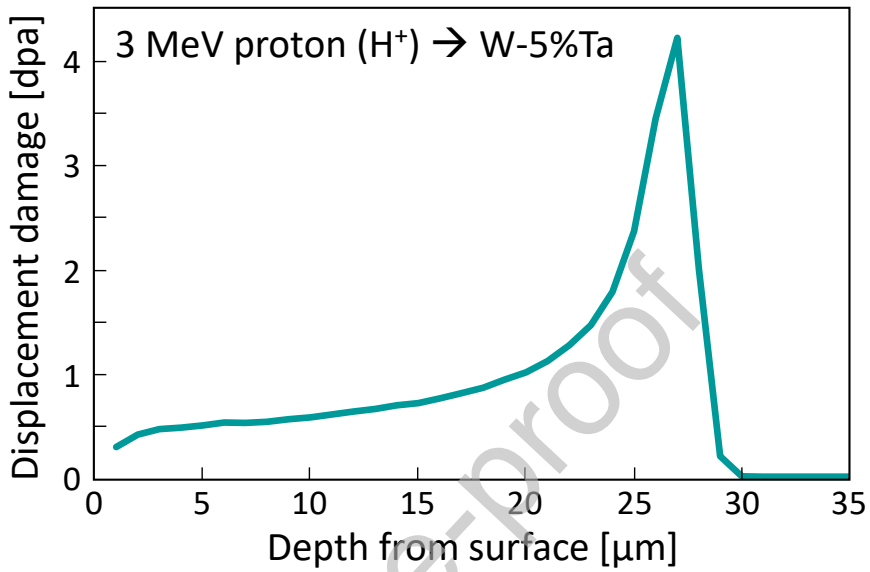

Fig. 3 Metallographic images after electrolytic polishing of (a) pure W, (b) W-1%Ta, (c) W-3%Ta, and (d) W-5%Ta in as-received condition.

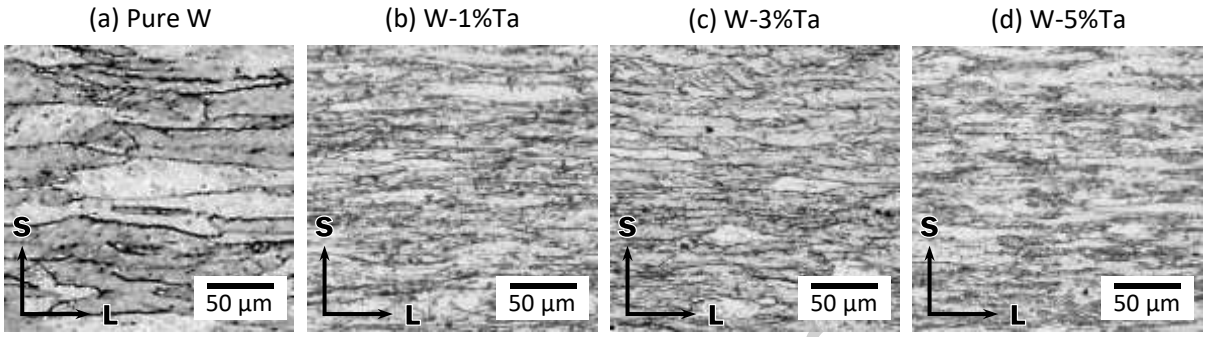

Fig. 4 Average grain sizes of pure W, W-1%Ta, W-3%Ta, and W-5%Ta in as-received condition. d_L and d_S are for sizes along L and S directions.

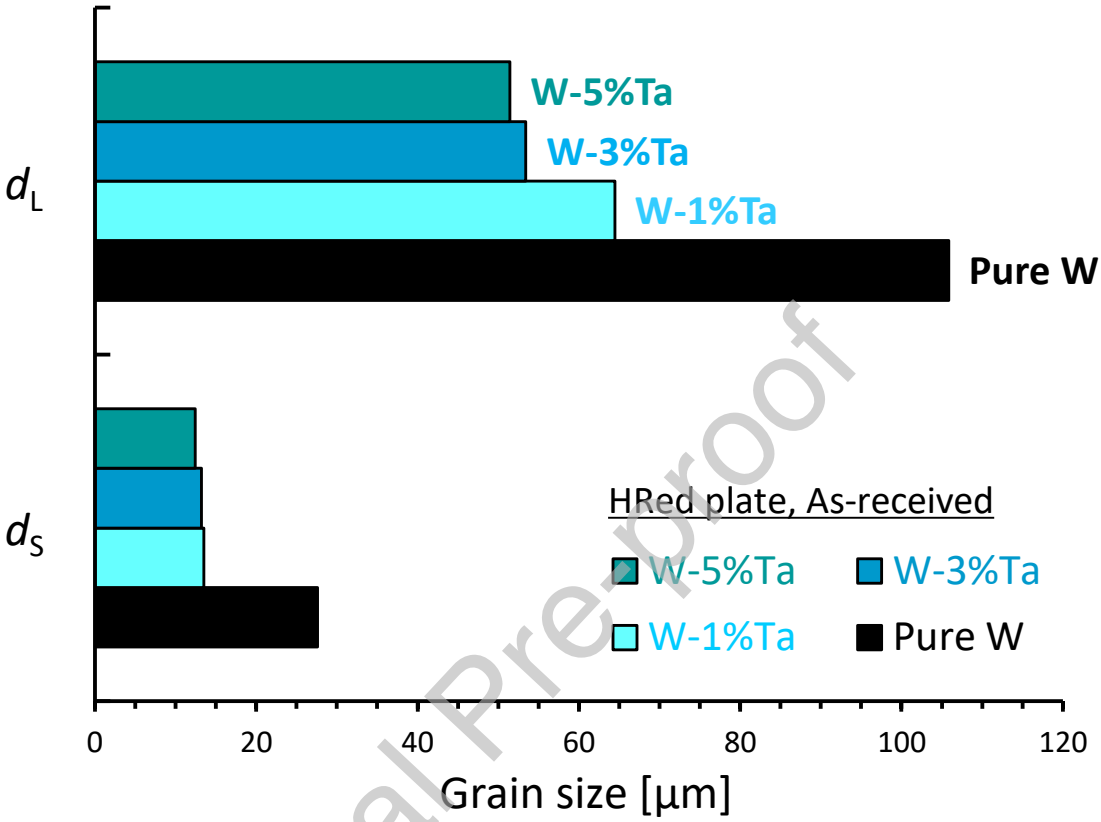

Fig. 5 TEM images of (a) pure W, (b) W-1%Ta, and (c) W-3%Ta in as-received condition.

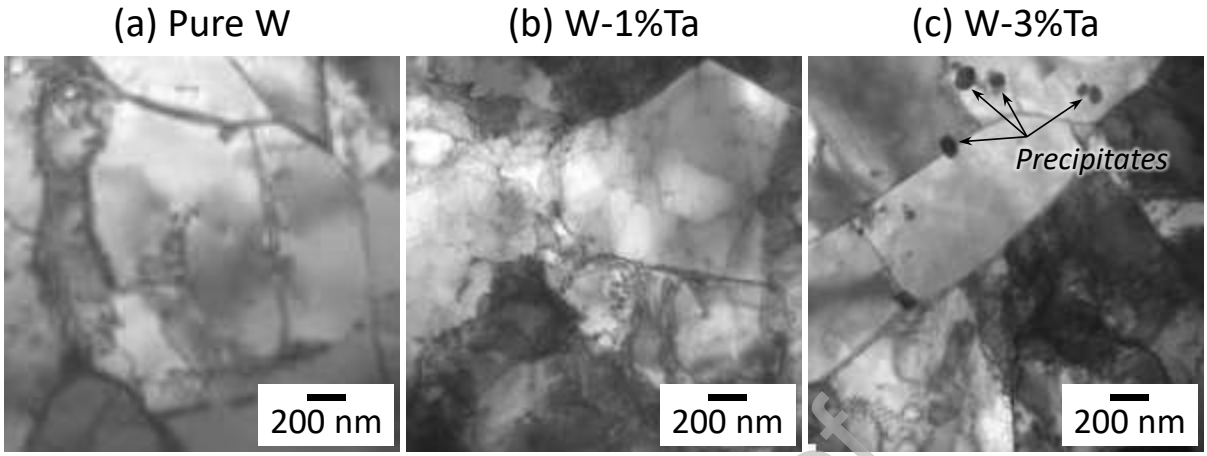

Fig. 6 Relationship between Ta concentration and lattice constant obtained by XRD analysis of pure W, W-1%Ta, W-3%Ta, and W-5%Ta in as-sintered condition. Theoretical relation calculated by the equation based on the Vegard's law is also plotted as dotted line [95].

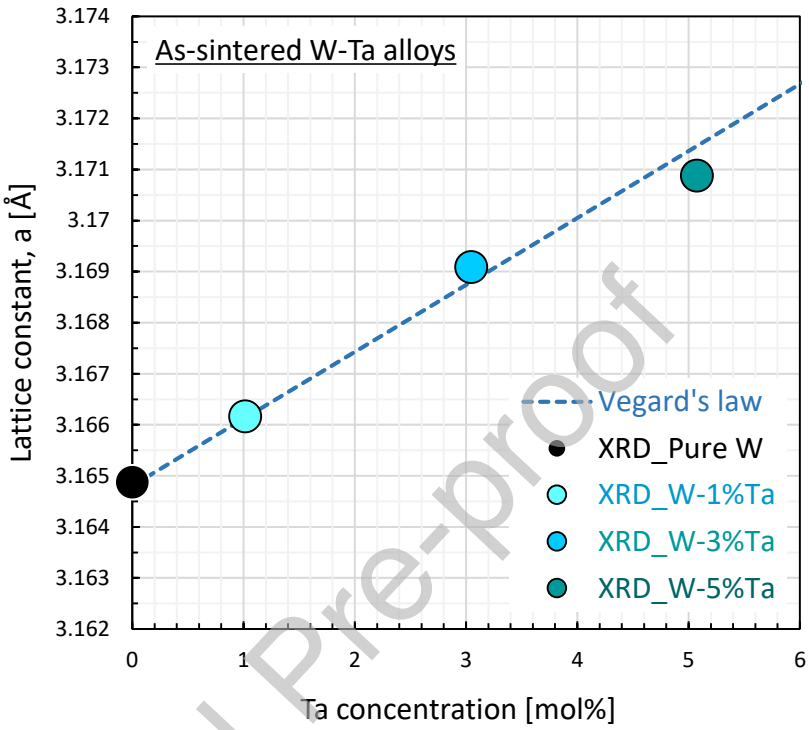

Fig. 7 (a) Vickers hardness after isochronal annealing for 1 h measured on L × S surface of pure W [49, 51, 53], W-1%Ta, W-3%Ta [81], and W-5%Ta. (b) Ta concentration dependences of recrystallization temperature determined by (a).

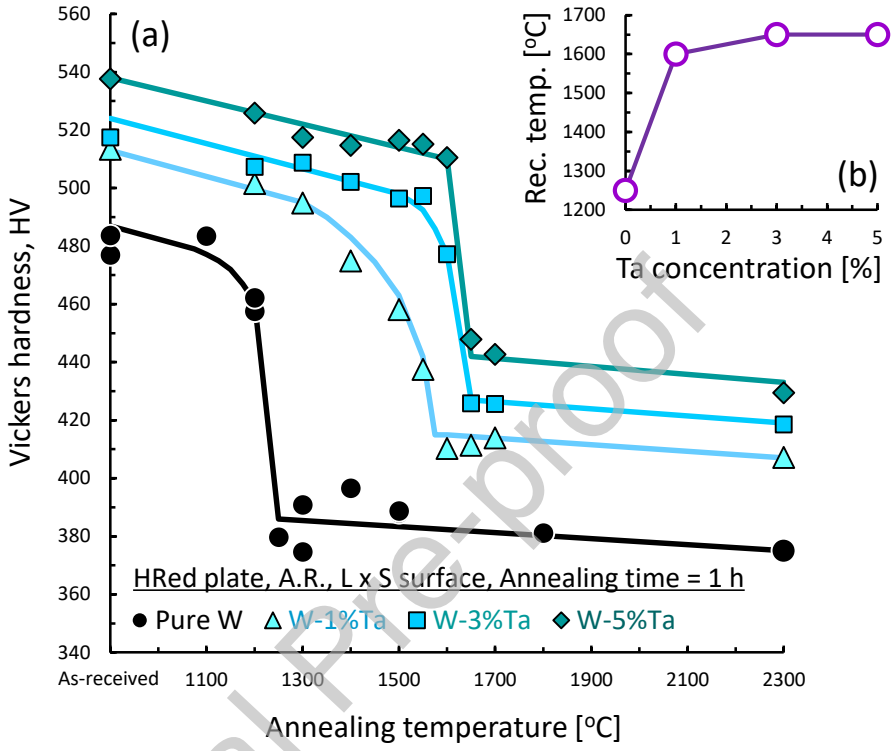

Fig. 8 Ta concentration dependences of (a) grain size along L and S directions (d_L and d_S), (b) cell size, and (c) Vickers hardness measured on L × S surfaces in as-received and recrystallized (annealed at 2300 °C for 1 h) conditions.

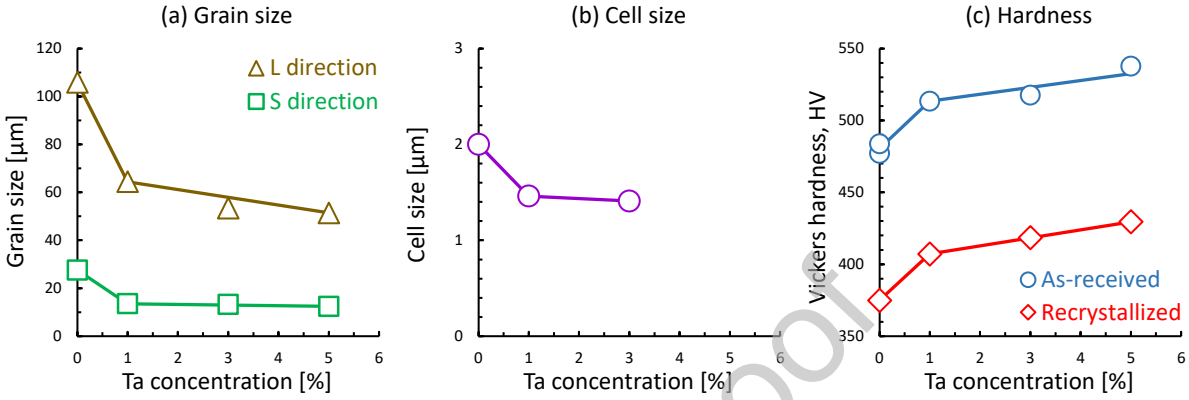

Fig. 9 (a) UTS, (b) $\sigma_{0.2}$, (c) TE, (d) RA, and (e) UE by tensile tests along L direction of pure W [38, 39, 49–51, 53], W-1%Ta, W-3%Ta [81], and W-5%Ta in as-received condition.

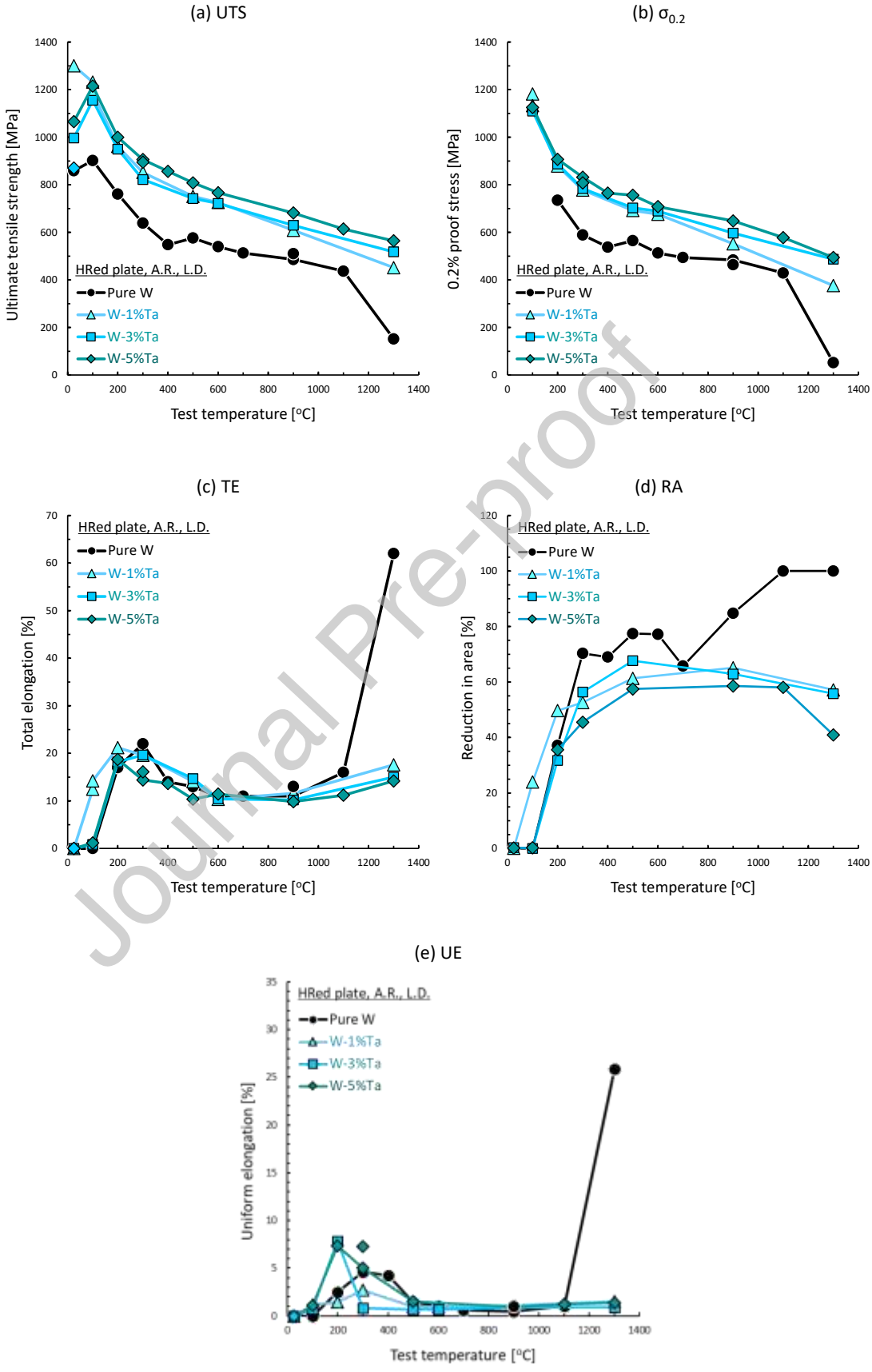

Fig. 10 Optical microscope images of test section of specimens after tensile tests along L direction of pure W, W-1%Ta, W-3%Ta, and W-5%Ta in as-received condition.

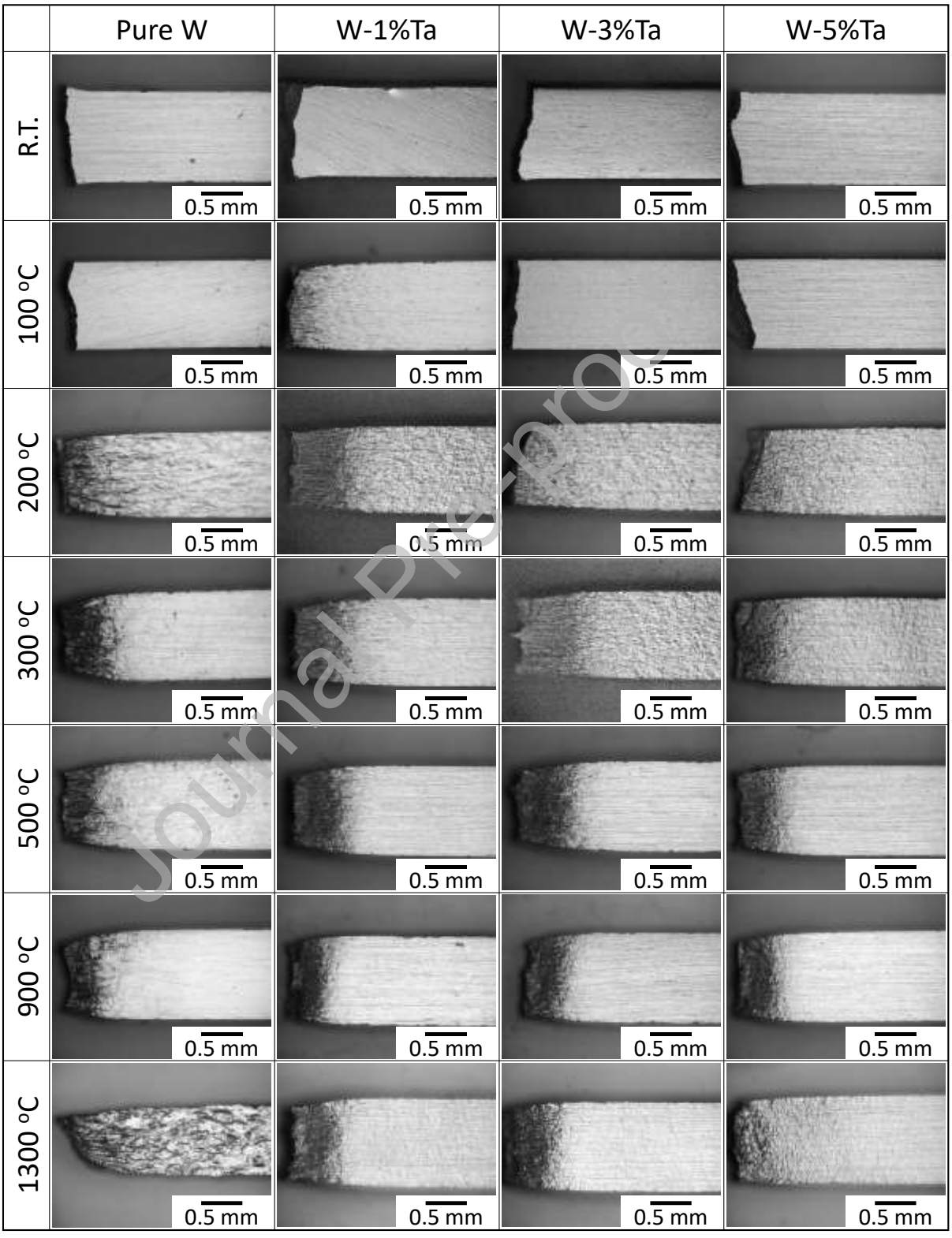

Fig. 11 SEM images of fracture surface after tensile tests along L direction of pure W, W-1%Ta, W-3%Ta, and W-5%Ta in as-received condition.

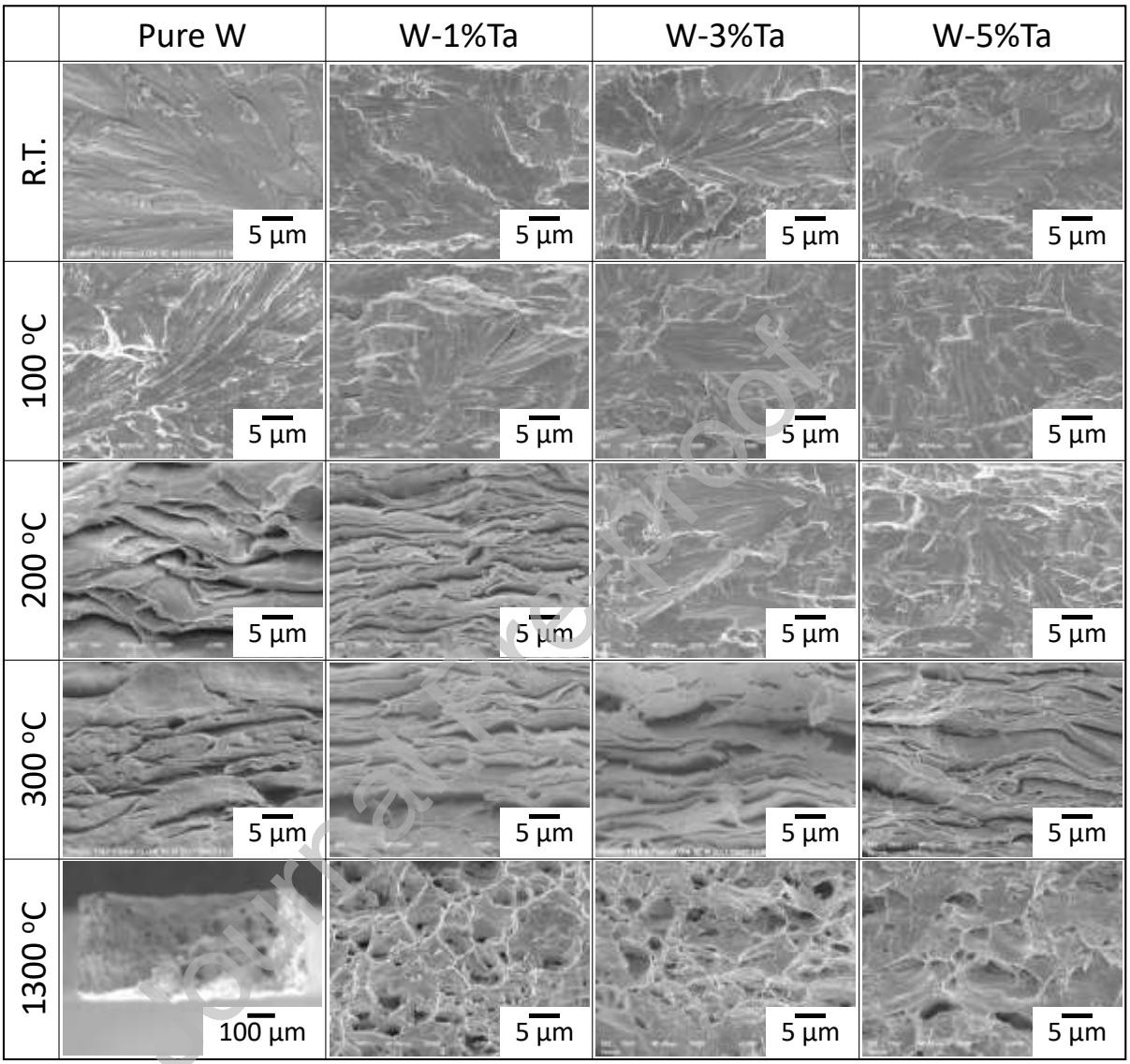

Fig. 12 Optical microscope images of test section of specimens after tensile tests at 1300 °C along L direction of W-1%Ta, W-3%Ta, and W-5%Ta in as-received condition.

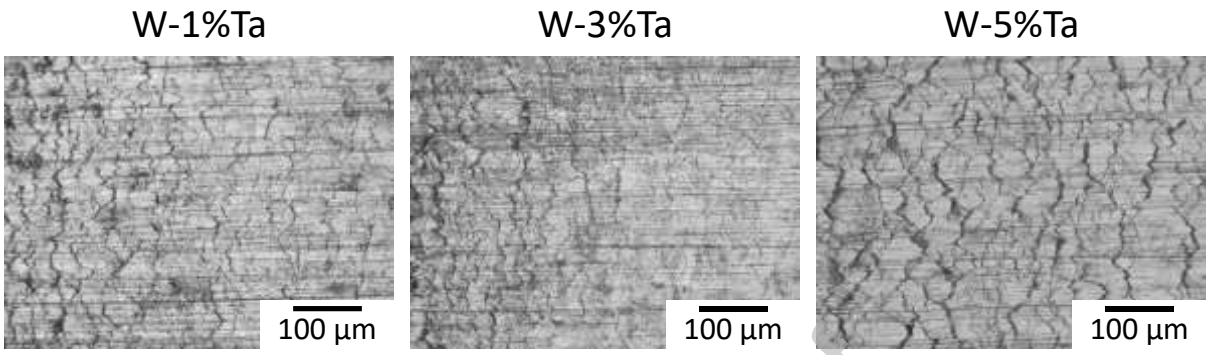

Fig. 13 Absorbed energy by Charpy impact tests along L-S direction of hot-rolled plates made of pure W, W-1%Ta, W-3%Ta, K-doped W, W-3%Re, and K-doped W-3%Re in as-received condition [46, 49–51, 53, 81] and forged round-blanks made of pure W, W-1%Ta, and W-5%Ta in as-received condition [77].

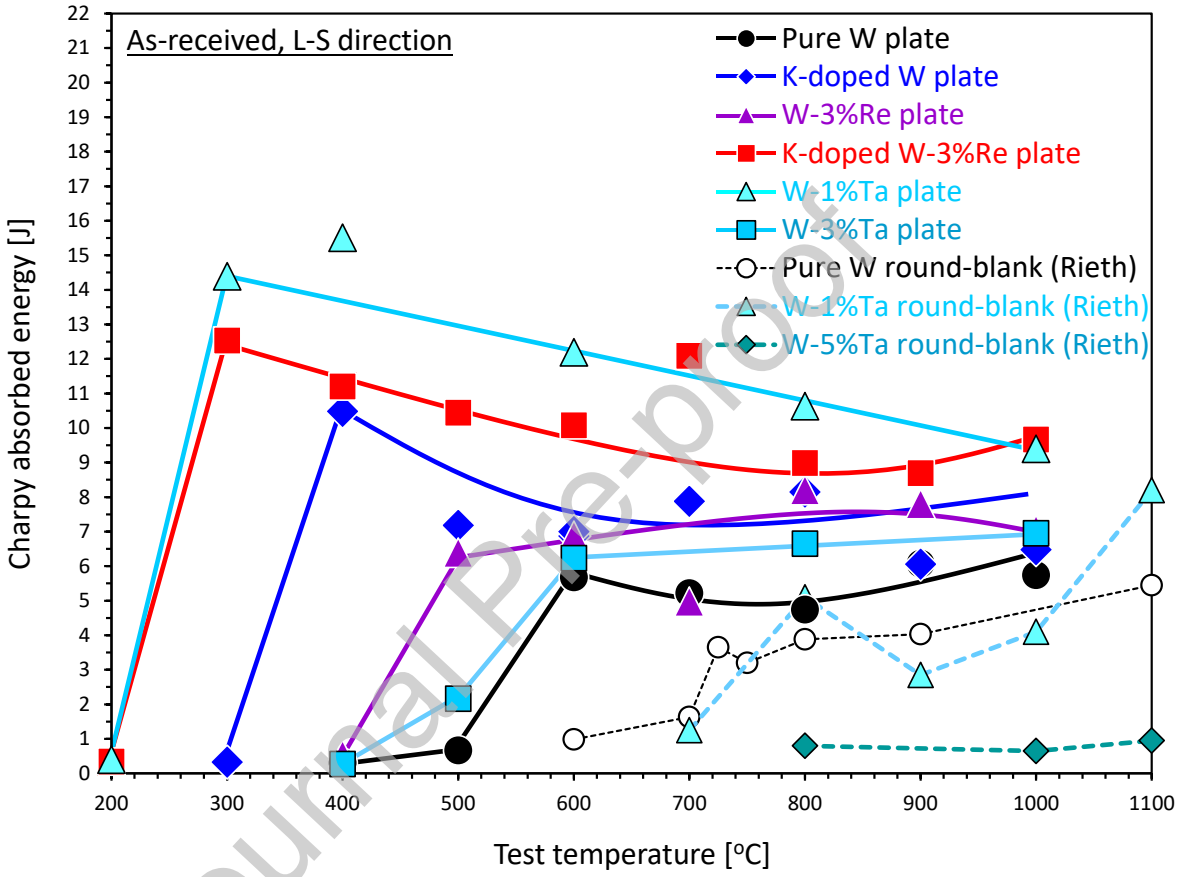

Fig. 14 Relationships between grain size along S direction (d_S) and (a) USE and (b) $DBTT_{Charpy}$ by Charpy impact tests along L-S direction of hot-rolled plates made of pure W (7 mm thick), pure W (4 mm thick), W-1%Ta, W-3%Ta, K-doped W, W-3%Re, and K-doped W-3%Re in as-received condition [46, 49–51, 53, 81, 100–103] and a forged round-blank made of pure W in as-received condition [77].

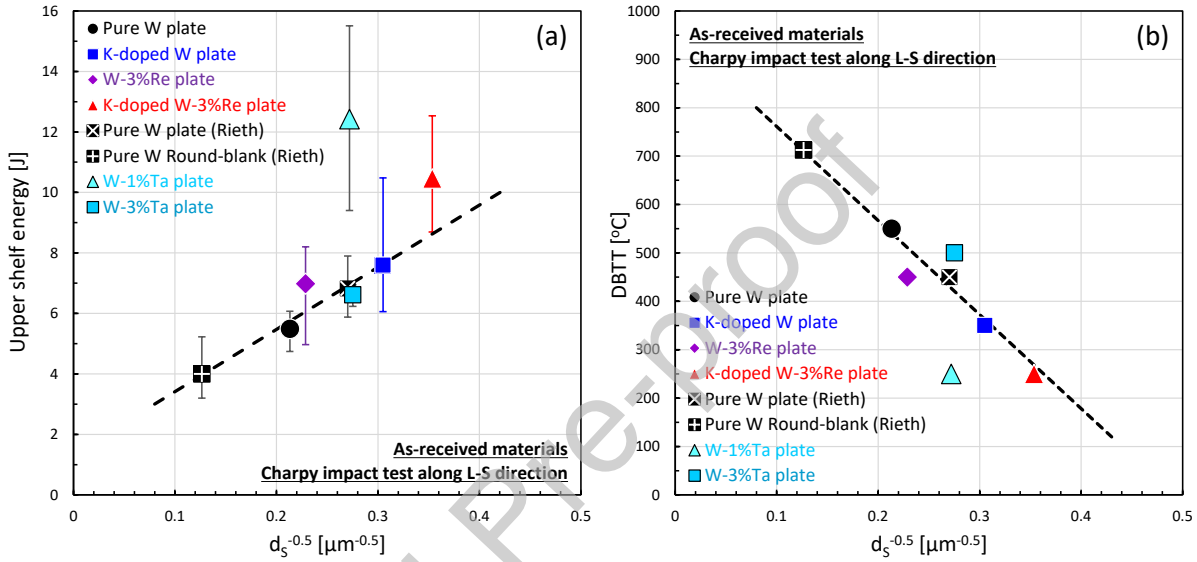

Fig. 15 Appearances of specimens made of hot-rolled plates after Charpy impact tests along L-S direction. (a) W-1%Ta at 400 °C, (b) K-doped W-3%Re at 500 °C, (c) W-3%Ta at 800 °C, (d) pure W at 800 °C, and (e) pure W at 600 °C (un-notched specimen with 3 mm × 3 mm × 27 mm) [46, 49–51, 53, 81].

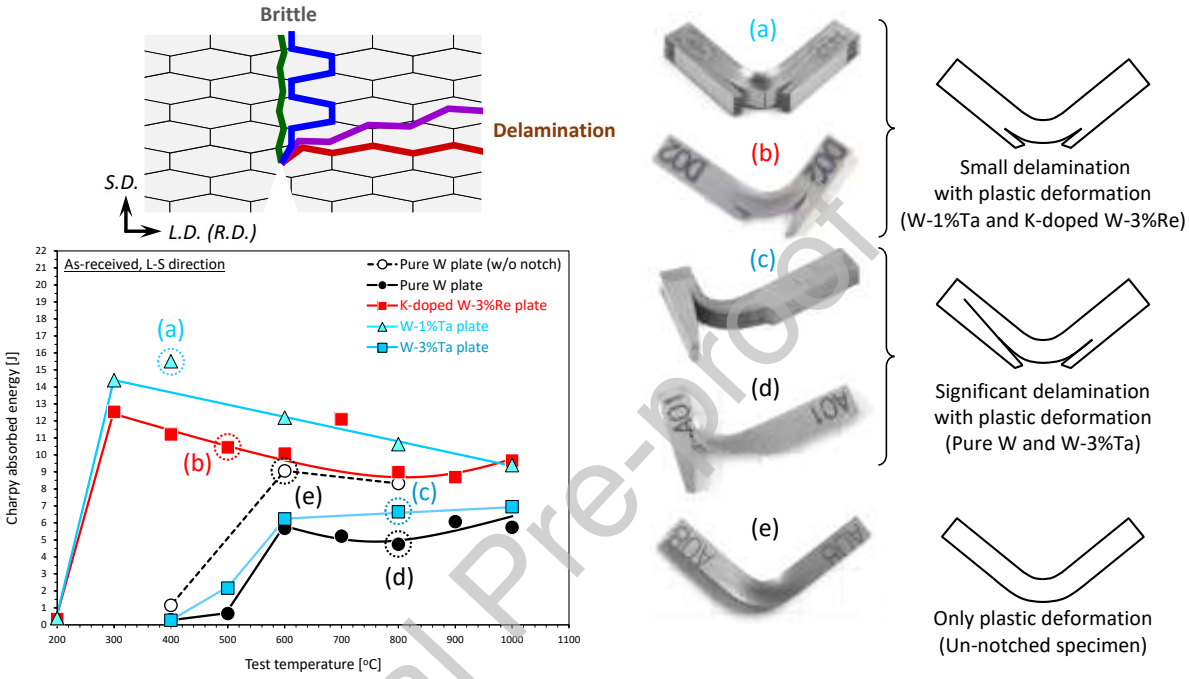

Fig. 16 Changes in Vickers hardness by 3 MeV proton irradiation at 1500 °C to 0.5 dpa of pure W, W-1%Ta, W-3%Ta, W-5%Ta, and W-3%Re in as-received and recrystallized (annealed at 2300 °C for 1 h) conditions. TEM images of pure W and W-5%Ta in as-received condition after proton irradiation are also shown.

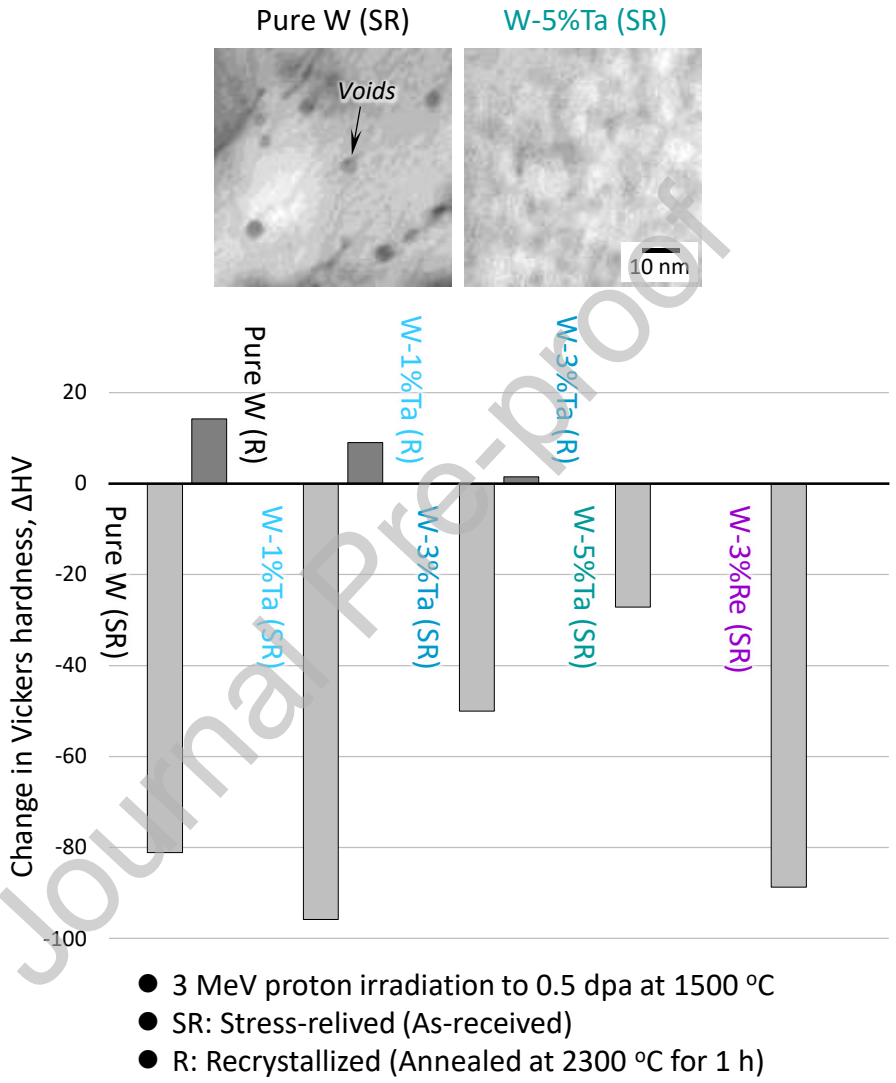

Fig. 17 Schematic illustration of temperature range from DBTT ($DBTT_{Tensile}$ and $DBTT_{Charpy}$) to recrystallization temperature by isochronal annealing for 1 h (T_{Rec}) of hot-rolled plates made of W-1%Ta, W-3%Ta, and W-5%Ta in the present study and pure W, K-doped W, W-3%Re, and K-doped W-3%Re in the previous study [53].

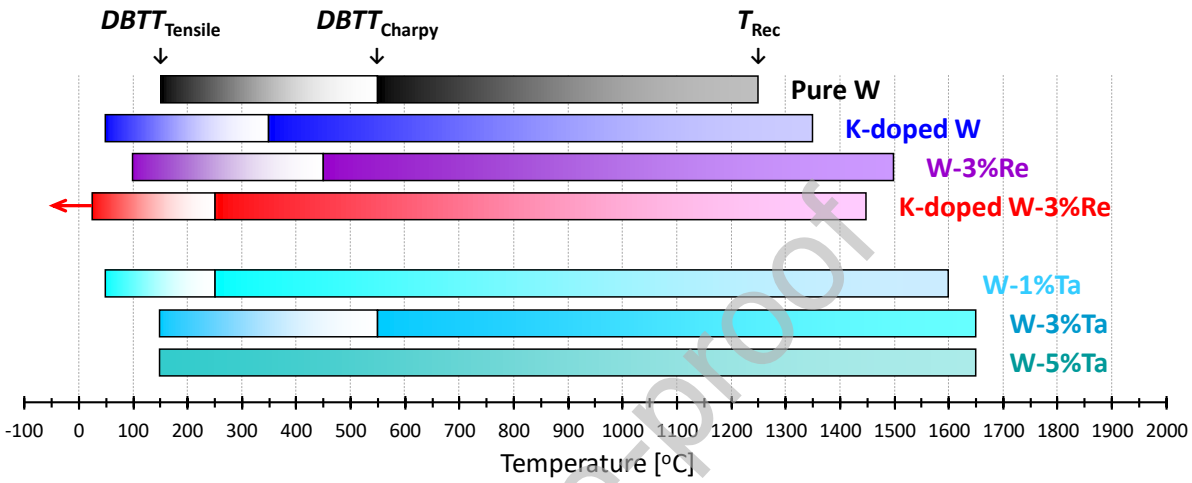

Fig. 18 Thermal diffusivity of pure W [44, 47], W-1%Ta, W-3%Ta, W-5%Ta, W-1%Re [47], and W-3%Re [47] in as-received condition.

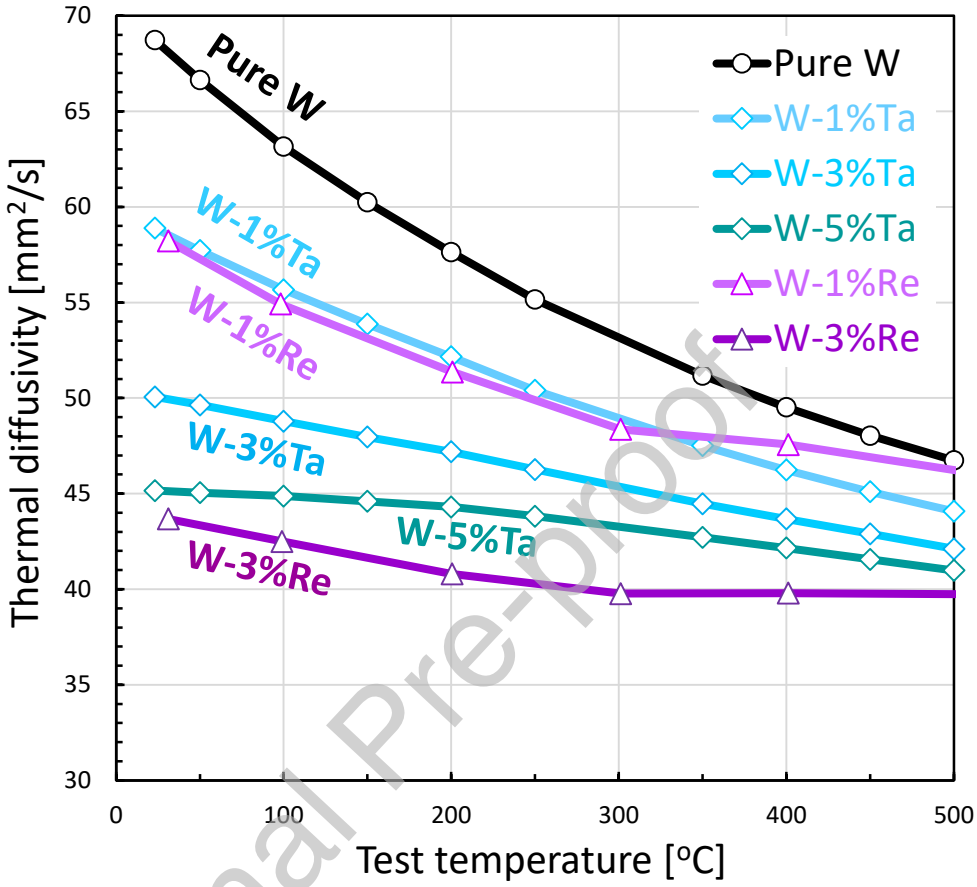

Fig. 19 SEM images of surface of pure W and W-3%Ta in as-received condition after thermal shock tests with background steady state D-plasma exposure. Arithmetic mean surface roughness, R_a, is shown in each image [81].

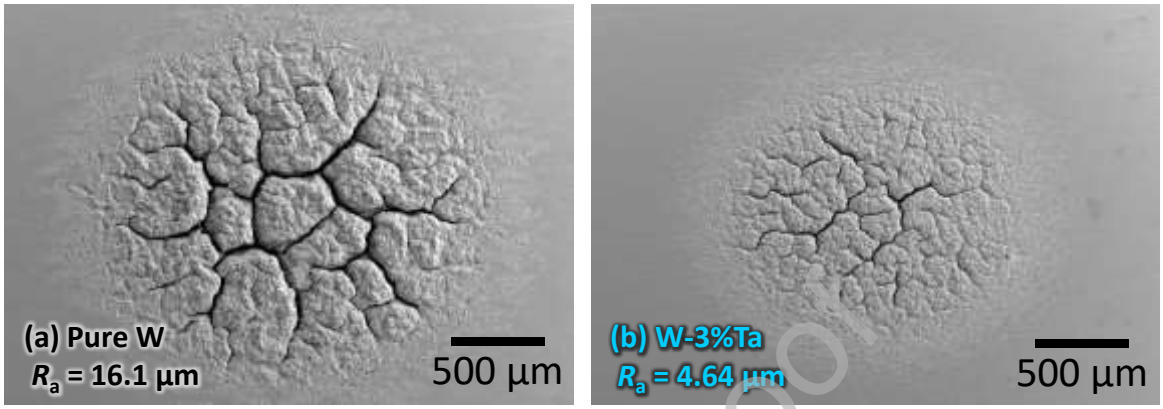

Devise: PSI-2 (FZJ), base temperature: 700 °C, number of laser pulse: 1×10^5,
laser power density: 0.38 GW/m^2, pulse duration: 0.5 ms, D-plasma fluence: 4.1×10^{25} m^{-2}